SIRT7 mediates L1 elements transcriptional repression and their association with the nuclear lamina

Berta Vazquez, Joshua Thackray, Nicolas Simonet, Sanjay Chahar, Noriko Kane-Goldsmith, Simon Newkirk, Suman Lee, Jinchuan Xing, Michael Verzi, Wenfeng An, et al.

7870–7885 *Nucleic Acids Research, 2019, Vol. 47, No. 15* *Published online 21 June 2019*
doi: 10.1093/nar/gkz519

SIRT7 mediates L1 elements transcriptional repression and their association with the nuclear lamina

Berta N. Vazquez[1,2,†], Joshua K. Thackray[1,†], Nicolas G. Simonet[3], Sanjay Chahar[1,4], Noriko Kane-Goldsmith[1], Simon J. Newkirk[5], Suman Lee[5], Jinchuan Xing[1], Michael P. Verzi[1], Wenfeng An[5], Alejandro Vaquero[2,3], Jay A. Tischfield[1] and Lourdes Serrano[1,*]

[1]Department of Genetics, Human Genetics Institute of New Jersey, Rutgers University, Piscataway, NJ 08854, USA, [2]Chromatin Biology Laboratory, Josep Carreras Leukaemia Research Institute, Badalona, Barcelona 08916, Spain, [3]Chromatin Biology Laboratory, Cancer Epigenetics and Biology Program (PEBC), Bellvitge Biomedical Research Institute (IDIBELL), Barcelona 08908, Spain, [4]Montpellier Institute of Molecular Genetics (IGMM), CNRS and the University of Montpellier, 34090, France and [5]Department of Pharmaceutical Sciences, College of Pharmacy and Allied Health Professions, South Dakota State University, Brookings, SD 57007, USA

Received March 13, 2019; Revised May 30, 2019; Editorial Decision June 02, 2019; Accepted June 03, 2019

ABSTRACT

Long interspersed elements-1 (LINE-1, L1) are retrotransposons that hold the capacity of self-propagation in the genome with potential mutagenic outcomes. How somatic cells restrict L1 activity and how this process becomes dysfunctional during aging and in cancer cells is poorly understood. L1s are enriched at lamin-associated domains, heterochromatic regions of the nuclear periphery. Whether this association is necessary for their repression has been elusive. Here we show that the sirtuin family member SIRT7 participates in the epigenetic transcriptional repression of L1 genome-wide in both mouse and human cells. SIRT7 depletion leads to increased L1 expression and retrotransposition. Mechanistically, we identify a novel interplay between SIRT7 and Lamin A/C in L1 repression. Our results demonstrate that SIRT7-mediated H3K18 deacetylation regulates L1 expression and promotes L1 association with elements of the nuclear lamina. The failure of such activity might contribute to the observed genome instability and compromised viability in SIRT7 knockout mice. Overall, our results reveal a novel function of SIRT7 on chromatin organization by mediating the anchoring of L1 to the nuclear envelope, and a new functional link of the nuclear lamina with transcriptional repression.

INTRODUCTION

Long interspersed elements-1 (LINE-1, L1) are non-LTR retrotransposons that hold the capacity of self-propagation through retrotransposition in mammalian genomes. L1s comprise ∼19% and 17% of the mouse and human genome, respectively (1,2), and are considered to be a major driving force of human genome evolution (3). A mammalian full-length L1 sequence includes an 5′ untranslated region (5′UTR) harboring an active promoter, two open reading frame proteins (ORF1p and ORF2p) necessary for L1 retrotransposition and the 3′ untranslated region (3′UTR) that contains a poly (A) tract. Most mammalian genomic L1 sequences are incapable of self-propagation due to mutations and truncations (1). L1 transcriptional activation has been reported during mammalian early embryogenesis and in germ cells (4,5,6), which led to the concept that L1 *de novo* retrotransposition might lead to germline and somatic mosaicism, reviewed in (7). Indeed, distinct L1 insertions have been reported among individual somatic cells such as in neurons (8,9,10,11). Whether this somatic genetic variability contributes to cell-specific functional determination or disease is still controversial. Undoubtedly, L1 activity has profound effects on gene expression. L1s participate in the formation of chimeric repeat-genic transcripts (12). L1s inserted in gene bodies might affect the quality and quantity of the mRNA transcript (13), and in a more global scale L1 transcriptional activation can affect the overall cellular pool of non-coding and coding RNAs (14). In addition, L1 retrotransposition often involves the transduction of 3′ nearby sequences (15,16), and the mobilization of other non-autonomous retrotransposons such as human

*To whom correspondence should be addressed. Tel: +1 848 445 9656; Email: serrano@biology.rutgers.edu
†The authors wish it to be known that, in their opinion, the first two authors should be regarded as Joint First Authors.

Alu sequences and murine B1 and B2 elements (17,18) potentially shuffling transcriptional regulatory regions. Moreover, active L1s can compromise genome integrity. The activity of the L1-encoded endonuclease generates DNA damage far above their retrotransposition potential promoting cell cycle arrest (19,20), induction of apoptosis (21) and cell senescence (22). Consistently, L1 activity is observed in cancer and aging cells (23,24). Whether L1 activity is the cause or the effect of these cellular degenerative processes is not clear. There are a few reported examples of L1 retrotransposition promoting insertional mutagenesis at tumor suppressor genes, which might precede oncogenic transformation (25,26,27).

The cell has developed multiple mechanisms of defense against L1 activity, ranging from small RNA-related machineries to restriction proteins acting at the post-translational level such as AID/APOBEC proteins reviewed in (28). Transcriptional silencing is predominantly mediated by epigenetic mechanisms involving the deposition of repressive histone post-translational modifications and by DNA methylation. These chromatin modifications vary depending on cell type and cell developmental stage. DNA methylation at L1 is established in early embryogenesis by *de novo* DNA methyltransferases (29) and is believed to be the main mechanism of L1 silencing in somatic tissues. Trimethylation of lysine 9 on histone H3 (H3K9me3), a characteristic epigenetic mark of constitutive heterochromatin, is present at the 5′UTR of intact L1 in both differentiated and undifferentiated cells (30). H3K9me3-mediated repression seems to be the primary L1 silencing mechanism in ESCs (31,32) and germ cells (30), which is mediated by the H3K9me3 methyltransferases Suv39h1/2 (31). In male germ lines, L1 repression is facilitated by P element-induced wimpy testis (Piwi)-interacting RNAs (piRNAs), which target L1 transcripts and facilitate the recruitment of the DNA and histone methyltransferases (30,33). For more ancient L1s, with plausibly limited transcriptional activity, H3K9me3 deposition is mediated by the DNA binding Krüppel-associated box domain-containing zinc finger proteins (KRAB-ZFPs) and their cofactor KAP1 (KRAB-associated protein 1) by promoting the recruitment of the methyltransferase SETDB1 (34). Other repressive marks characteristic of facultative heterochromatin such as trimethylated H4K20 and H3K27 found at different subfamilies of endogenous retrovirus did not show a uniform pattern of enrichment on L1s in ESCs (35). Analysis of L1 repression in somatic tissues from aging and cancer cells reveal additional epigenetic mechanisms of L1 silencing such as histone lysine deacetylation, which is correlated with a closer or inaccessible repressive chromatin state. In cancer cells, deacetylated histones decorate the chromatin of newly L1 insertions (36) and the use of histone deacetylases (HDACs) inhibitors is sufficient to induce L1 reactivation (36,37). The specific HDACs responsible for L1-associated chromatin deacetylation are not known.

Overall, L1s are vulnerable to the progressive loss of heterochromatin that characterize cancer and aging cells, such as progressive CpG island hypomethylation and loss of histone methylation and deacetylation (38,39,40,41). Indeed, L1 sequences are an important part of the mammalian cell heterochromatic content. Euchromatin and heterochromatin are compartmentalized in the eukaryotic nucleus. Heterochromatin is predominantly found at the nuclear exterior associated with elements of the nuclear envelope such as components of the nuclear lamina (42,43,44,45). Indeed, the anchoring of chromatin to the nuclear lamina is important for gene silencing and the maintenance of expression programs (46). Transcriptional activation disrupts associations with the nuclear lamina (47,48) and alternatively, the tethering of genes to the nuclear lamina promotes their repression (49,50). L1 elements are enriched in Lamini-associated domains (43,51). However, whether L1-Lamin association is necessary for L1 transcriptional repression is not known.

Here we report that SIRT7, a member of the mammalian sirtuin family of deacylases and ADP ribosylases, participates in the epigenetic regulation of L1 repression genome-wide in both mouse and human cells. ChIP-seq analysis shows that the majority of chromatin-associated SIRT7 binds L1 elements where it regulates H3K18Ac levels. Mechanistically, SIRT7-mediated H3K18 deacetylation promotes the association of L1 with lamin proteins. Importantly, association of L1 sequences to the nuclear lamina is indispensable for their transcriptional repression. Accordingly, SIRT7 depletion is correlated with increased L1 expression and retrotransposition.

MATERIALS AND METHODS

Cell lines and treatments

Mouse embryonic fibroblasts (MEFs) were isolated from WT and *SirT7*$^{-/-}$ mice as previously described (52). K562 cells were obtained from ATCC (CCL-121) and HT1080 were kindly provided by Dr Brenemann. Cells were transfected by electroporation as described previously (53). Briefly, 1×10^7 cells were resuspended in 250 μl of Ingenio buffer (Mirus) and were electroporated with 1 μM of SCR, SIRT7 or Lamin A/C siRNA using a BioRad device (Gene Pulser Xcell) with 4 mm gap cuvette (BioRad) at 200 V and 950 μF. Electroporated cells were then transferred to complete medium and incubated at 37°C for 48 h before harvesting. MEF cells were transfected with an Amaxa Nuclefactor System (for details, see 'Retrotransposition Assay' section) or infected with retroviral particles as described previously (54).

Plasmids

SIRT7-, SirT7H188Y-, H3K18WT-, H3K18Q- and H3K18R-pMSCV vectors were established as described previously (53). Human HA-Lamin A was cloned into the pcDNA4/TO vector (Invitrogen). The pWA125 and pWA126 retrotransposition plasmids were kindly provided by Dr Ann, and are both based on a synthetic mouse L1 element (55) (i.e. ORFeus-Mm) and contain a GFP-based retrotransposition reporter. The pWA126 vector contains two mutations that abolish the endonuclease and reverse transcriptase activities and is used as a control for background GFP signal. pMSCV-GFP was generated in (56). pMD7-5′UTR-Fluc described in detail in Luciferase assay section of 'Materials and Methods'. SCR siRNA was

obtained from SIGMA and SIRT7 and Lamin siRNA were obtained from Dharmacon.

Chromatin immunoprecipitation

ChIP was carried out as previously described (53). Briefly, samples were crosslinked in 1% formaldehyde for 10 min at 37°C, washed twice with PBS and then collected from dishes. For SIRT7, ChIP was carried out with nuclear extracts. First, cells were resuspended in Lysis Buffer 1 (5 mM HEPES, 85 mM KCl, 0.5% NP-40) and incubated for 5 min on ice to disrupt cellular membranes. After centrifugation, nuclei were resuspended in Lysis Buffer 2 (1% SDS, 10 mM EDTA, 50 mM Tris and protease inhibitors) and incubated on ice for 40 min. For H3K18Ac and Lamin A/C ChIP, whole cell extracts were obtained by directly lysing cells in Lysis Buffer 2 for 40 min on ice. Chromatin was then sonicated to an average fragment size of 150–300 bp as analyzed by agarose gel electrophoresis, and subjected to immunoprecipitation with anti-SIRT7, anti-H3K18Ac or anti-LaminA/C antibodies (see Supplementary Table S1 for details). ChIPs were washed five times with ice-cold RIPA buffer (1% NP-40, 0.7% Na deoxycholate, 50 mM Tris, 1 mM EDTA, 500 mM $LiCl_2$, pH 8.0), crosslinks were reversed (1% SDS, 0.1 M $NaHCO_3$; 6 h at 65°C) and DNA was purified (minElute PCR Purification Kit, Qiagen). Finally, the concentration of ChIP and INPUT DNA was measured using PicoGreen (Life Technologies). For Quantitative PCR, GAPDH and LINE elements were analyzed with 1 ng and 50 pgr of ChIP and INPUT DNA, respectively. See Supplementary Table S2 for primer sequences.

Library preparation and ChIP-sequencing

ChIP libraries were prepared using a ThruPlex DNA-seq library preparation Kit (Rubicon Genomics) following the manufacturer's protocol. ChIP libraries were then size selected with PippinPrep (Sage Science) for a final library fragment size of 350–400 bp, and quantified with KAPPA qPCR. ChIP libraries were then sequenced on a HiSeq 2500 (Illumina) with 2 × 100 bp paired-end reads to a depth of $>20 \times 10^6$ fragments per sample at the RUCDR, Infinite Biologics sequencing center (Rutgers University, NJ). Reads were de-multiplexed and concatenated, and delivered as fastq files.

ChIP-seq analysis

Raw read quality was first assessed with fastqc (version 0.11.3, Babraham Bioinformatics). FastQC: a quality control tool for high-throughput sequence data (available online at: http://www.bioinformatics.babraham.ac.uk/projects/fastqc), followed by adapter clipping and quality trimming with Trimmomatic version 0.36 (57). Reads were then aligned to the mouse (UCSC mm9) or human (UCSC hg19) reference genomes with Bowtie with options –n 2 –k 10 (58), and converted to BAM format with Samtools (59). ChIP and alignment quality was evaluated computing library complexity (PBC), FRiP, insert size and strand cross-correlation analysis. All samples passed the ENCODE quality standards for ChIP-seq studies. Peak calling was performed using MACS version1.4.2 (60), and RPKM-normalized signal files were generated from BAM data using DeepTools version 2.4.2 (61). Repetitive element annotations for the mm9 and hg19 reference genomes were obtained from repeatmasker (RepeatMasker Open-4.0. 2013–2015 <http://www.repeatmasker.org>), and were processed to defragment elements based on their ID field. Intersection of ChIP peaks with repetitive elements was performed with the Bedtools package version 2.17.0 (62). Classification of ChIP peak genomic context was performed with CEAS version 0.9.9.7 (63). Heat map and average profile plots were generated using in-house scripts utilizing metaseq version 0.5.6 (64), pybedtools version 0.6.9 (65) and Matplotlib version 2.0.2 (Zenodo. http://doi.org/10.5281/zenodo.573577). Individual profile plots were generated using IGV version 2.3.98 (66). PhastCon scores (30-way vertebrate) against the mm9 reference genome were obtained from UCSC (67,68), and average profiles were generated with in-house scripts. SIRT7 peak proximity to TSS elements was computed with GREAT v2.0.2 (69) using the mm9 reference genome and default settings. Alignment of ChIP-seq reads to L1 consensus sequences was performed using bowtie2 v2.2.6. L1 consensus sequences obtained from repbase (70,71) were first indexed with bowtie2-build using default options followed by alignment of ChIP-seq reads using bowtie2 with options –N 1 –local. ChIP signal over the length of the consensus sequence was then plotted using in-house scripts, with data expressed as the $\log_2$ ratio of ChIP divided by Input after adjustment for library sizes. Data shown are from replicate #1 from two independent concordant replicates for both human and mouse.

RNA extraction and quantitative RT-PCR

Cultured cells and tissues were homogenized in TriReagent® (Invitrogen) and RNA was isolated with a Direct-zol™ RNA Kit (Zymo Research) according to the manufacturer's instructions. About 1.5 μg of RNA was then digested with DNase I (Invitrogen), purified with an RNAeasy kit (Qiagen) and subjected to cDNA synthesis using the High Capacity cDNA Reverse Transcription Kit (Applied Biosystems) with random hexamers and poly-dT according to manufacturer's instructions. For 5′RACE qPCR, cDNA was generated using a SMARTer RACE Kit (Clontech Laboratories). cDNA generated without the SMARTer II Oligonucleotide was used as a negative control. PCR products were cloned into the pGEM-TEasy vector (Promega). DNA sequencing was performed on an ABI PRISM 377 DNA sequencer (Applied Biosystems). Real-Time PCR was performed using SYBR Green (Applied Biosystems) in an ABI 7900HT real-time PCR machine. Reactions were run in triplicate with an initial denaturation step at 95°C for 10 min, followed by 40 cycles of denaturation at 95°C for 15 s and annealing/elongation at 60°C for 1 min and a final melting curve analysis to verify amplification specificity. The housekeeping gene β-Actin was used as an internal control to normalize expression levels and reactions without the addition of reverse transcriptase were performed in parallel as negative controls. The primer sequences are provided in Supplementary Table S2.

Retrotransposition assays

WT and *SirT7*$^{-/-}$ primary MEFs cells were transfected with pWA125 or pWA126 retrotransposition vectors (see Supplementary Figure S9A for more details), and with the pMSCV-GFP transfection efficiency control vector using the Amaxa P4 Primary Cell 96-well Nucleofector Kit (Lonza) according to the manufacturer's instructions. Briefly, 10^5 cells were resuspended in 20 μl of the Nucleofector Solution together with 500 ng of plasmid DNA and were electroporated in a 96-well Shuttle Nucleofector with the program setting 96-CZ-167. Transfected cells were then transferred to cell culture dishes with pre-warmed complete DMEM and treated 24 h post-transfection with puromycin (Sigma-Aldrich) at a final concentration of 1 μg/ml. Cells were harvested 7 days post-transfection. The number of EGFP positive cells and the mean fluorescence intensity of GFP$^+$ cells was quantified by flow cytometry using FACScalibur (Beckman Coulter) and analyzed with Flow Jo 7/8 (Tree Star).

Protein immunoprecipitation

Lamin A/C antibody (#abcam, ab8984) was first conjugated to protein A and protein G magnetic beads (Life Technologies) according to manufacturer's instructions. Chromatin fractions from 293 cells were obtained as previously described (54). Briefly, cells were first lysed in Hypotonic Buffer (10 mM Tris:HCl pH 7.9, 1.5 mM $MgCl_2$, 10 mM KCl, 0.1 mM PMSF, 0.5 mM DTT and protease inhibitors) for 10 min at 4 °C to break the cellular membrane. After centrifugation, protein supernatant was discarded, and cellular pellet was resuspended in RIPA buffer (50 mM Tris:HCl, pH 7.4, 150 mM NaCl, 2 mM EDTA, 1% NP-40, 0.1% SDS; 0.1 mM PMSF, 0.5 mM DTT and protease inhibitors) to obtain nuclear extracts. Nuclear extracts were treated with benzonase (SIGMA) according to manufacturer's instructions, and the protein supernatant was incubated with anti-Lamin A/C beads overnight at 4 °C. Protein complexes were washed three times with ice-cold BC-100 washing buffer (20 mM Tris:HCl, pH 8.0, 100 mM KCl, 10% glycerol, 1 mM EDTA, 1 mM DTT, 0.1% Nonidet P-40; 0.1 mM PMSF and Protease inhibitors), and elution was performed by incubating the beads 10 min with 25 μl of 0.1 M glycine, pH 2.8. About 25% of the eluted protein complexes and 1% of the INPUT were then resolved on NuPAGE 4–12% Bis-Tris gel (Invitrogen) and analyzed by western blot using anti-SIRT7 and anti-LaminA/C (Cell Signaling, 2032) antibodies.

Micrococcal nuclease assay

Three 10-cm dishes of *SirT7*$^{-/-}$ and WT MEFs were grown to 80–90%confleunce. About 10–15 × 10^6 cells of each genotype were resuspended in 1 ml of lysis buffer (10 mM Tris, 10 mM NaCl, 3 mM $MgCl_2$, 1% of NP-40, pH 7.5) and incubated on ice for 10 min. Nuclei were collected by centrifugation at 300 × *g* for 5 min at 4°C. The nuclear pellet was then resuspended in 400 μl of nuclear lysis buffer (20 mM Tris, 20 mM KCl, 70 mM NaCl, 3 mM $CaCl_2$ and protease inhibitor cocktail, pH 7.5). Aliquots of 60 μL were then treated with 4 Units of micrococcal nuclease (MNase, Thermo Fischer) and digested at 37°C for 0, 1.5, 3, 5, 10 and 15 min, respectively. Then 3 μl of 0.5 M EDTA was added to stop digestion, and DNA was purified by using the NucleoSpin® Gel and PCR Clean-up procedure (Macherey-Nagel). About 500 pgr of DNA was used for qPCR analysis using SybrGreen (ThermoFisher). Primers were designed to target the promoters of the L1MdA consensus sequence and the B-globin gene to obtain PCR amplicons longer than the length of a single nucleosome. Specifically, amplicons were 248 and 350 bp long for the B-globin and L1Mda promoters, respectively. Mononucleosomes formed as the result of MNase digestion cannot be amplified by qPCR. Therefore, reduced amplification indicates more MNase digestion, which is interpreted as the presence of more accessible/open chromatin at the assayed loci.

Luciferase assay

We generated a stable HCT-116-5′UTR-Fluc cell line carrying an integrated 5′UTR-Fluc transgene (pMD7), which expresses the firefly luciferase (Fluc) reporter under the human L1RP 5′UTR promoter (Genebank accession #AF148856.1). pMD7 was constructed through three cloning steps. First, pMD2 was derived from the Sleeping Beauty transposon cloning vector pT2BH (72) by double digestion with SalI and XhoI and subsequent religation. Second, the Fluc reporter under SV40 promoter was released from pGL4.13 (Promega) as a EcoRV/BamHI fragment, and ligated into EcoRV/BglII digested pMD2, making pMD3. Third, the SV40 promoter in pMD3 was replaced with L1RP 5′UTR promoter by ligating the 5′UTR from pJCC5-RPS (73) as a EcoRV/NcoI fragment with EcoRV/NcoI digested pMD3, making pMD7. To make the stable cell line, 90 000 HCT-116 cells were seeded in a 24-well plate, and 24 h later cotransfected with 100 ng of pMD and 20 ng of SB100X (72) using FuGENE HD reagent. Cells were harvested 24 h post transfection and reseeded into 96-well plates at the density of 0.8 cells/well. Single cell clones showing Fluc activity were retained for downstream analysis. For luciferase assays, a total of 10.000 HCT-116-5′UTR-Fluc cells were plated in triplicate into a 96-well plate and transfected with 200 mM Scr or SirT7 siRNA (Dharmacon) using Fugene reagent (Promega). Seventy-four hours after transfection, cell viability was measured using Sensilite (PerkinElmer) and luciferase activity with Luciferase Assay System (Promega).

Pull-down assays

The following histones peptides were synthesized by AnaSpec (San Jose, CA): Histone H3 (1–21) (Cat# AS-61702) [ARTKQTARKSTGGKAPRKQLA-GG-K(BIOTIN)-NH2], Histone H3K18ac (1–21) (Cat#AS-64638) [ARTKQTARKSTGGKAPR-K(Ac)-QLA-GGK(Biotin)-NH2], Histone H3K18me2 (1–21) (Cat#AS-64620) [ARTKQTARKSTGGKAPR-K(Me2)-QLA-GGK(Biotin)-NH2]. Pull-down assays were performed with Streptavidin agarose beads purchased from Millipore (#16-126). Preparation of the peptide-bound resin and peptide pull-down from nuclear extracts were performed

as described (54). Briefly, HA-Lamin A/C purified from HEK-293F cells was incubated with the respective streptavidin bound biotin labeled peptide for 12 h at 4°C (salt concentration adjusted to 150 mM of KCl in presence of 0.1% Triton X-100). The streptavidin agarose beads were washed five times with 10 volumes of PBS/0.1%Triton X-100 and finally eluted with 1 volume of 2× Laemmli buffer. The amount of HA-Lamin A/C pulled-down was detected by western blot using anti-HA antibody, while a dot blot with anti-biotin was performed as loading control. See Supplementary Table S1 for antibodies sources.

FISH and imaging

For single locus FISH, BACs were obtained from CHORI (RP24-286G19 and RP24-184M19) and were amplified and isolated using standard techniques. Probes were generated by incorporation of modified nucleotides (aa-dUTP, Sigma) via nick translation and coupled to fluorophores with the ARES kit (Invitrogen) following manufacture's instructions. For L1 probe FISH, probes were generated via PCR incorporating biotin-dUTP using primers designed against the L1MdT family of L1 elements. Specifically, primers for this probe were designed against the L1MdT consensus sequence (RepBase) with amplicons generated starting from the internal 5′ UTR through the length of the ORF2 region. PCR reactions were run partially substituting dTTP with biotin-dUTP (1:3 ratio), and using WT MEF genomic DNA as template. All PCR reactions were subjected to size selection via agarose gel electrophoresis with a target window of 200–500 bp (see Supplementary Table S2 for primer sequences). Probes were combined in an equimolar ratio, in addition to mouse Cot-1 (BAC probes only) and sheared salmon sperm DNA (Invitrogen) for blocking, precipitated and resuspended in hybridization buffer. Probes were applied to cells grown on coverslips that were fixed and processed for FISH. Slides were denatured for 3.5 min at 75°C, followed by incubation at 37°C for 1–2 days. Slides were then washed 3 × 10 min with 2X SSC at 37°C, then 3 × 10 min with 0.1× SSC at 62°C. For L1 probe FISH, biotin was detected using anti-biotin primary antibody and visualized with secondary antibody coupled to fluorophore (see Supplementary Table S1 for antibodies sources). Finally, slides were counterstained with DAPI and mounted with slowfade gold mounting media (Invitrogen).

For all FISH experiments, images were acquired using a LSM510 META confocal microscope (Carl Zeiss) equipped with a Plan-Apochromat 100×/1.46 NA oil immersion lens. 3D reconstruction and image analysis were performed using Imaris software (Bitplane, A.G.). Nuclei were segmented based on DAPI staining intensity using the standard *Surfaces* function of Imaris software. For single locus FISH, hybridization signals were located and modeled using the *Spots* module, which detects the hybridization signal center of mass. These coordinates were used to compute the radial position of each hybridization signal relative to the nucleus. For L1 probe FISH (see Supplementary Figure S5), the relative radial position of each voxel within each nucleus was computed and the average L1 probe intensity along the nuclear radius, which was divided into 20 bins, was measured. To compute the relative radial position of an arbitrary point within a given nucleus, we used the library geometry3Sharp (https://github.com/gradientspace/geometry3Sharp) to generate 3D AABBTrees representing the isosurface mesh used to segment each nucleus. We then query this tree to find a point on the surface that lies on the ray originating at the center of the nucleus and passing through the point of interest. We define the radial position for this point as the ratio of distances: $distance(center, point) / distance(center, surface)$. All images among all samples within a given experiment were acquired and quantified using the same microscope and analysis parameters. Correlation metrics were computed as previously described (56). Additional reagents details can be found on Supplementary Tables S1 and S2.

RESULTS

SIRT7 preferentially binds to active families of LINE-1 elements

We used chromatin immunoprecipitation (ChIP) followed by high-throughput DNA sequencing (ChIP-seq) to identify SIRT7-binding sites throughout the genome in primary MEFs. Bioinformatic analysis of the data revealed that SIRT7 binds 72 622 loci scattered across the genome (Figure 1), and that these binding sites are highly conserved between species (Supplementary Figure S1A). The majority of SIRT7 binding sites are located within intergenic regions and only ∼2% are found within promoter and exonic regions (Figures 1A and Supplementary S1B). Strikingly, 80% of SIRT7-binding sites were found at L1 elements (Figure 1B). The binding of SIRT7 at L1 elements was further confirmed by ChIP coupled to quantitative PCR (ChIP-qPCR) and compared with SIRT7 occupancy at selected genomic regions (Figure 1C). SIRT7 is enriched at the ribosomal gene 28S consistent with the role of SIRT7 in rDNA transcription regulation (74), but dramatically increased (15-fold) at L1 loci relative to a negative control locus (GAPDH). The alignment of the SIRT7 ChIP-seq reads to the consensus mouse L1 sequence indicates that SIRT7 binding is present throughout the L1 (Supplementary Figure S1C). Importantly, our results reveal that SIRT7 specifically binds the most recently evolved and therefore, putatively active families of L1 elements (Figure 1D). Moreover, SIRT7 occupancy at L1 elements genome-wide was also present in K562 human cell line but to a lesser extent (Supplementary Figure S2A). Similar to mouse cells, SIRT7 in this human cell line preferentially binds the most recently evolved families of L1 elements (Supplementary Figure S2B).

SIRT7 promotes the association of L1 elements to Lamin A/C

Previous reports have shown that L1 elements are enriched at Lamin-associated domains (LADs) (44,51), a transcriptional repressive nuclear compartment (46). Strikingly, analysis based on our own and previously published data (GSE36132 (44)) showed an enrichment of lamin proteins to all L1 elements as indicated by a positive Lamin-DamID score, which was dramatically increased in the subset of L1 elements bound by SIRT7 (Figure 2A). Consis-

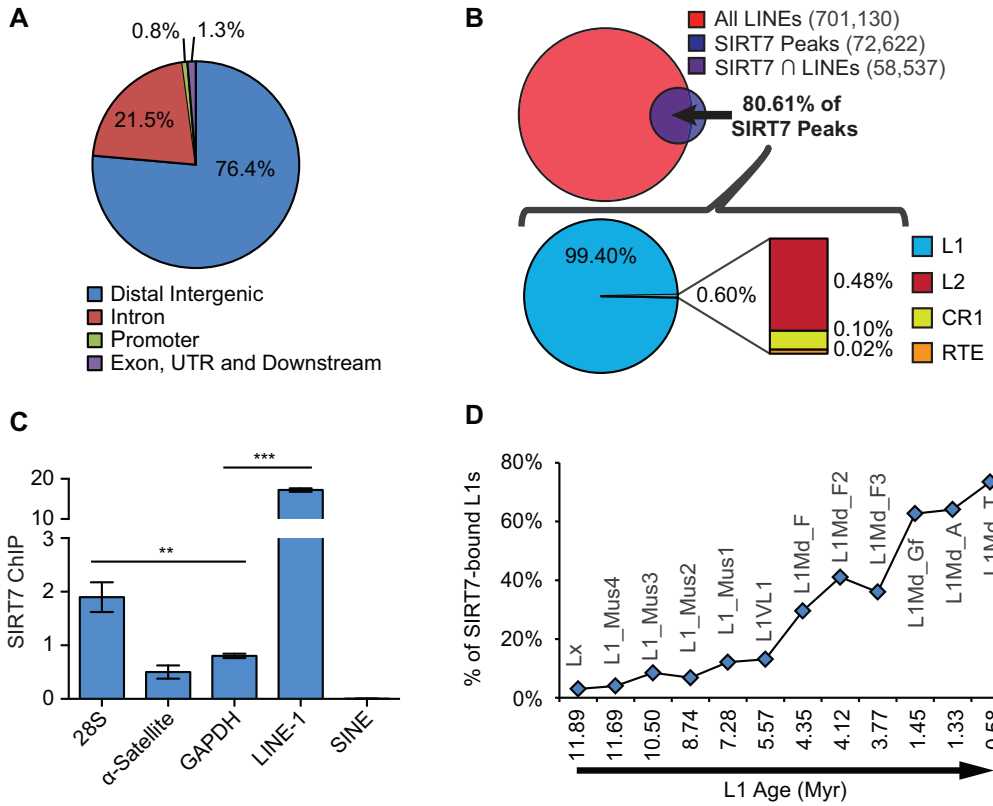

Figure 1. SIRT7 binds L1 elements genome-wide. (**A**) Genomic distribution of SIRT7-binding sites in MEFs categorized by genomic features. (**B**) Venn diagram (top) showing the number of SIRT7 peaks that intersect with all LINEs genome-wide. Pie chart (bottom) showing the family classification of LINEs occupied by SIRT7 in MEFs. Data indicate the percentage of family in the set of all LINEs occupied by SIRT7. Genomic LINE annotations were obtained from RepeatMasker, and intersections computed with BEDTools. (**C**) ChIP-qPCR analysis showing SIRT7 occupancy in MEFs at the indicated genomic regions. All samples were normalized to input DNA (**$P < 0.01$; ***$P < 0.001$ by ANOVA single factor). (**D**) Relative occupancy of SIRT7 at the indicated L1 subfamilies in MEFs. Data represent the percentage of L1 elements in the indicated L1 subfamilies that are occupied by SIRT7. L1 subfamilies were organized according to their evolutionary age, from the oldest to the youngest, as reported in (89).

tently, endogenous SIRT7 and Lamin A/C are able to be co-purified by immunoprecipitation in MEFs cells (Figure 2B and Supplementary Figure S3). Importantly, we observed that Lamin A/C association with L1 elements is reduced in SIRT7-depleted cells (Figure 2C), despite similar levels of Lamin A/C between *SirT7*$^{-/-}$ and WT cells (Figure 2D). In addition, the reduced presence of Lamin A/C at L1 loci in SIRT7-deficient cells was directly dependent on SIRT7 deacetylase activity. Viral-mediated transduction of *SirT7*$^{-/-}$ MEFs with an active SIRT7, but not with a catalytically inactive SIRT7 point mutant, rescued Lamin A/C levels at L1 elements (Figure 2C). Collectively, these data suggest a functional interplay between SIRT7 and Lamin A/C in L1 regulation.

It is well documented that the anchoring of chromatin to the nuclear lamina is important for gene transcriptional repression (46). Similarly, SIRT7-mediated L1 repression might involve the anchoring of L1 elements to the nuclear lamina. To test this possibility, we performed fluorescence *in situ* hybridization (FISH) targeting selected L1 loci in WT and *SirT7*$^{-/-}$ cells (Figure 2E and F). We first used two BACs probes: one within a LAD enriched for SIRT7-occupied L1 elements and an adjacent non-LAD control locus devoid of SIRT7-bound L1 elements (Figure 2E). Probe coordinates, based on weighted centers of each fluorescence signal, were used to calculate the relative radial distance to the nuclear surface. Although the overall distribution was not statistically different according with Kolmogorov–Smirnov (KS) testing, we computed the correlation coefficient between the WT and *SirT7*$^{-/-}$ radial distributions for both probes (LAD rho = 0.9549 with 95% CI [0.816, 0.989] versus Non-LAD rho = 0.9932 with 95% CI [0.971, 0.998]), which shows a decreased correlation of the relative positional frequency in the LAD locus as compared to the Non-LAD locus. In addition, we observed a significant decrease in the frequency of the most peripheral positioning of the LAD locus in *SirT7*$^{-/-}$ cells compared to WT cells, while no significant changes in the nuclear localization of the adjacent non-LAD probe were observed between both cell types. To further discern the impact of SIRT7 in L1 nuclear spatial distribution, we designed a L1 FISH probe spanning the consensus sequence of the L1MdT family of L1 elements with the rationale that the vast majority of these L1 family members are occupied by SIRT7 (Figure 1D). After hybridization of this probe on primary WT and *SirT7*$^{-/-}$ MEFs followed by confocal 3D imaging analysis (Supplementary Figure S5), we observed that the majority of the FISH signal in WT cells was found at the nuclear periphery (Figure 2F, left and Supplementary Figure S6). This is consistent with previous reports placing ~60%

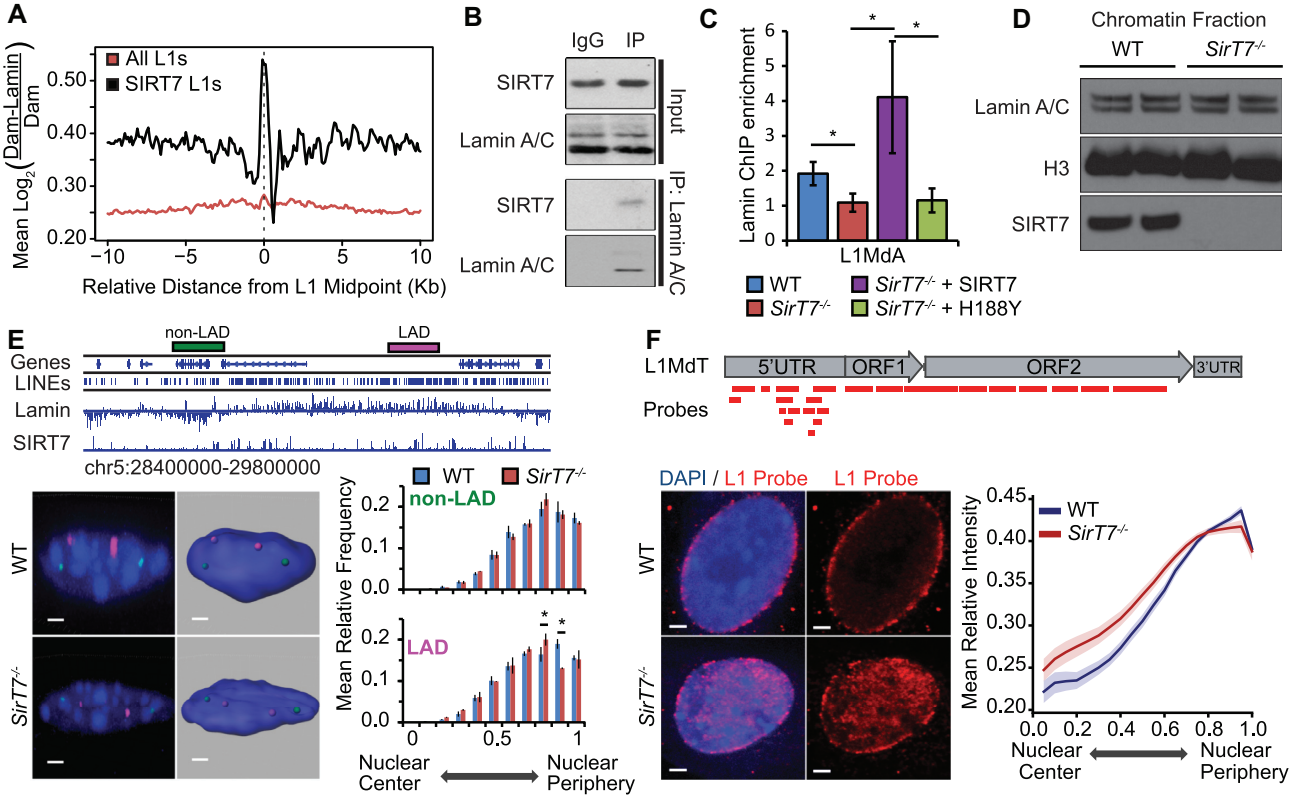

Figure 2. SIRT7 is required for the tethering of L1 elements to the nuclear lamina. (**A**) SIRT7 peaks are located in regions with higher LaminB1 DamID score. Lamin B1 DamID score tracks in MEFs were obtained from (43). Average score profiled over SIRT7-associated L1 elements (black) and at all L1 elements (red). (**B**) Endogenous Lamin A/C was immunoprecipitated from 293 whole cell extracts and probed for Lamin A/C and SIRT7. (**C**) ChIP-qPCR of L1 in WT and *SirT7*$^{-/-}$MEFs, and upon overexpression of SIRT7 WT or catalytically inactive point mutant SIRT7-H188Y in *SirT7*$^{-/-}$ MEFs, using an anti-Lamin A/C antibody. Data are normalized to input DNA and GAPDH. (**D**) Detection of Lamin A/C and SIRT7 from WT and *SirT7*$^{-/-}$ MEFs by western blot. H3 was used as a loading control. (**E**) (Top) Schematic showing genomic BAC probe placement and its association with genes, LINEs, Lamin B1, and SIRT7 signal. (Bottom) FISH analysis showing nuclear localization of probes targeting a LAD and a non-LAD region in WT and *SirT7*$^{-/-}$cells. (Bottom left) 3D reconstruction and rendering of the nuclear volume based on DAPI staining (blue), and BAC fluorescence signal was performed using IMARIS software from confocal *Z* stacks (scale bar = 2 μm). (Bottom right) BAC coordinates based on weighted centers of each fluorescence signal were used to calculate radial distance to the nuclear surface. (**F**) FISH analysis of the nuclear distribution of L1MdT family. (Top) Schematic representation of L1MdT consensus sequence annotated with location of FISH probes. (Left) Representative images (scale bar = 2 μm). (Right) L1MdT probe intensity plotted against nuclear radial position, where 0 indicates the nucleus center point and 1 indicates the nuclear periphery ($n = 50$ cells per genotype). Data represent mean ± SEM of three independent experiments per condition except otherwise indicated; $^{*}P < 0.05$ by ANOVA single factor.

of LINE elements in LAD regions (44). Quantification of the L1 probe intensity per voxel in relation to their relative nuclear radial position revealed a mild but significant decrease in the mean intensity at peripheral locations (0.8–1.0) and an increase in the central compartment (0.0–0.8) in *SirT7*$^{-/-}$ cells compared to WT (Figure 2F, right). In addition, WT nuclei showed a higher correlation of radial position and L1 probe intensity compared to *SirT7*$^{-/-}$ nuclei (rho = 0.907 ± 0.022 versus rho = 0.776 ± 0.045, respectively. *P*-value of 0.0108 by ANOVA). Taken together, our results indicate that L1 nuclear distribution becomes disrupted upon SIRT7 depletion and support a model where SIRT7 regulates the anchoring of L1 elements to the nuclear periphery.

SIRT7 regulates H3K18 acetylation levels at L1 loci

SIRT7 is known to be a NAD^{+}-dependent deacetylase of lysine 18 of histone H3 (H3K18). Acetylation of this residue has been previously described to be enriched at enhancers and promoters of active genes (75). Consistently, SIRT7-mediated H3K18 deacetylation at the promoters of a specific set of genes has been shown to lead to their silencing (76,77). We hypothesized that SIRT7-mediated H3K18 deacetylation has a broader role in transcriptional regulation considering the predominant occupancy of SIRT7 at L1 elements (Figure 1B). This hypothesis is further supported as SIRT7 catalytic activity is necessary to restore L1 association with the nuclear lamina in *SirT7*$^{-/-}$ MEFs (Figure 1C). To test this hypothesis, we performed ChIP-seq to determine H3K18Ac levels genome-wide in WT and *SirT7*$^{-/-}$ MEFs. ChIP-seq analysis of H3K18Ac enriched chromatin from WT MEFs corroborated previous reports of H3K18Ac occupancy. H3K18Ac is found at the peaks of H3K27Ac and H3K4me1 histone modifications that are enriched enhancers, and at promoters marked by the presence of H3K4me3 and the binding of RNA Polymerase II Subunit A (Supplementary Figure S4). Importantly, the levels of H3K18Ac at enhancers and promoters of canonical genes did not change significantly between WT and

SirT7$^{-/-}$ cells, consistent with our observation that SIRT7 is generally not enriched at these sites (Figure 1A). However, we observed that H3K18Ac is enriched at L1 elements occupied by SIRT7, and that SIRT7 deficiency resulted in a significant increase of H3K18Ac levels at these loci (Figure 3). SIRT7 specifically binds the most recently evolved and DNA sequence-intact families of L1 elements, such as the L1MdA family (Figure 1D). Consistently, the effect of SIRT7 on H3K18ac levels is bigger in Figure 3B, in which the average enrichment profile is over L1MdAL1 elements, as compared with Figure 3A that represents the H3K18ac average levels over all L1 elements. Moreover, knockdown of SIRT7 in HT1080 cells also resulted in a significant increase of H3K18Ac levels at L1 elements (Figure 4A) indicating that SIRT7 modulation of H3K18Ac levels at L1 elements also holds in human cells.

Histone H3K18 acetylation levels modulate Lamin A/C interaction with chromatin

Previous reports indicate that the association of sirtuins with components of the nuclear lamina impacts their enzymatic activities. Lamin A interaction with both SIRT1 and SIRT6 activates, albeit by an unknown mechanism, their deacetylase activity (78,79). To test whether SIRT7-Lamin A/C interplay could impact SIRT7 deacetylase activity at L1 elements, we measured H3K18Ac levels at L1 sequences in control and Lamin A/C knockdown cells by ChIP-qPCR (Figure 4A). We observed that, relative to control cells, depletion of Lamin A/C did not cause H3K18Ac levels at L1 loci to change significantly. However, depletion of SIRT7 led to a significant increase in H3K18Ac enrichment, consistent with our observations in WT and *SirT7*$^{-/-}$ -derived mouse cells (Figure 3).

To directly test whether SIRT7-mediated H3K18 deacetylation was necessary for Lamin A/C recruitment to L1 elements, we transduced WT and *SirT7*$^{-/-}$ cells with histone H3 mutants in which K18 was mutated either to glutamine (K18Q) or to arginine (K18R) to mimic an acetylated or deacetylated lysine residue, respectively. Overexpression of the H3K18Q mutant in WT cells resulted in a significant reduction of Lamin A/C levels at L1 elements measured by ChIP-qPCR. Conversely, overexpression of the H3K18R mutant in *SirT7*$^{-/-}$ cells increased Lamin A/C levels (Figure 4B). Interestingly, we were able to detect via western blot a dramatic reduction of Lamin A/C levels in the chromatin fraction of WT cells overexpressing the H3K18Q mutant, suggesting an effect of this histone acetylation status in other chromatin loci outside L1 (Figure 4C). Altogether these results indicate that SIRT7-mediated H3K18 deacetylation at L1 is not affected by SIRT7–Lamin A/C association but seems to be necessary for Lamin A/C recruitment to L1.

Taken together, these results support that SIRT7-mediated H3K18 deacetylation is critical for Lamin A/C-L1 element association. Structural analysis of Lamin A/C protein indicates that Lamin A/C is able to directly bind chromatin (80). To test whether the association of Lamin A/C with chromatin is impaired by the presence of H3K18Ac, we used biotinylated H3 peptides with K18 in an unmodified, acetylated or di-methylated state to pull-down purified Lamin A protein (Figure 4D and E). Our results indicate that Lamin A is able to directly bind the H3 histone tail peptide, and importantly, that acetylation of K18 reduces this interaction. Intriguingly, H3K18me2 peptides (peptide control) were also able to reduce Lamin A interaction. However, it is difficult to evaluate the biological relevance of this result as the role of H3K18 methylation has not been defined yet. Nevertheless, this observation strengthens the idea that modification of the H3K18 residue alters Lamin binding to chromatin. Overall, these results suggest that in the absence of SIRT7, H3K18 hyperacetylation prevents the association of L1 elements with the nuclear lamina by interfering with Lamin A/C binding to chromatin.

Increased LINE-1 expression and retrotransposition in the absence of SIRT7

Collectively, our results reveal an unanticipated and novel functional interplay between SIRT7 and Lamin A/C and suggest that SIRT7 may promote L1 repression via its interaction with the nuclear lamina. We first determined whether SIRT7 activity promotes L1 transcriptional silencing by measuring L1 expression levels in MEFs isolated from WT and *SirT7*$^{-/-}$ sibling mouse embryos. We observed a significant upregulation of L1 transcripts in *SirT7*$^{-/-}$-derived MEFs compared to WT cells (Figure 5A). Moreover, several tissues from *SirT7*$^{-/-}$ mice also displayed L1 deregulation (Figure 5A), being more predominant in those tissues where SIRT7 is highly expressed and become dysfunctional upon SIRT7 depletion (53,74,77,81,82). Importantly, the single copy gene *TBP*, which is devoid of any transcriptionally competent L1 element or SIRT7-binding sites, had similar levels of L1 expression between WT and KO cells from all tissues that we investigated. These results indicate that SIRT7 maintains the repression of more recently evolved, and therefore putatively active, L1 elements, consistent with the relative enrichment of SIRT7 at different L1 families (Figure 1D and Supplementary Figure S2B). Most importantly, transcriptional silencing of L1 elements was directly dependent on SIRT7 activity because viral-mediated transduction of *SirT7*$^{-/-}$ MEFs with an active SIRT7 was sufficient to repress L1 expression by 65% (Figure 5B). In addition, we generated a human colon carcinoma cell line with integrated firefly luciferase reporter cassette driven by the by a sense 5′UTR promoter derived from the human L1RP instance. Our results showed increased expression of the L1 construct in siRNA-mediated *SirT7* knockdown cells as compared with cells transfected with scramble siRNA (Figure 5C). Taken together, these results indicate that SIRT7 deficiency results in increased L1 expression across multiple mice tissue types and in human cells. Moreover, overexpression of the H3K18Q mutant histone resulted in a significant increase of L1 expression (Figure 5D) indicating that modulation of H3K18Ac levels at L1 elements regulates L1 transcription. Importantly, knockdown of Lamin A/C resulted in the transcriptional upregulation of L1 loci occupied by SIRT7 (Figure 5E). Although overexpression of the deacetylated K18 mutant histone (H3K18R) was sufficient to reduce L1 expression as compared to control cells, this reduction did not occur in the absence of Lamin A/C (Figure 5F).

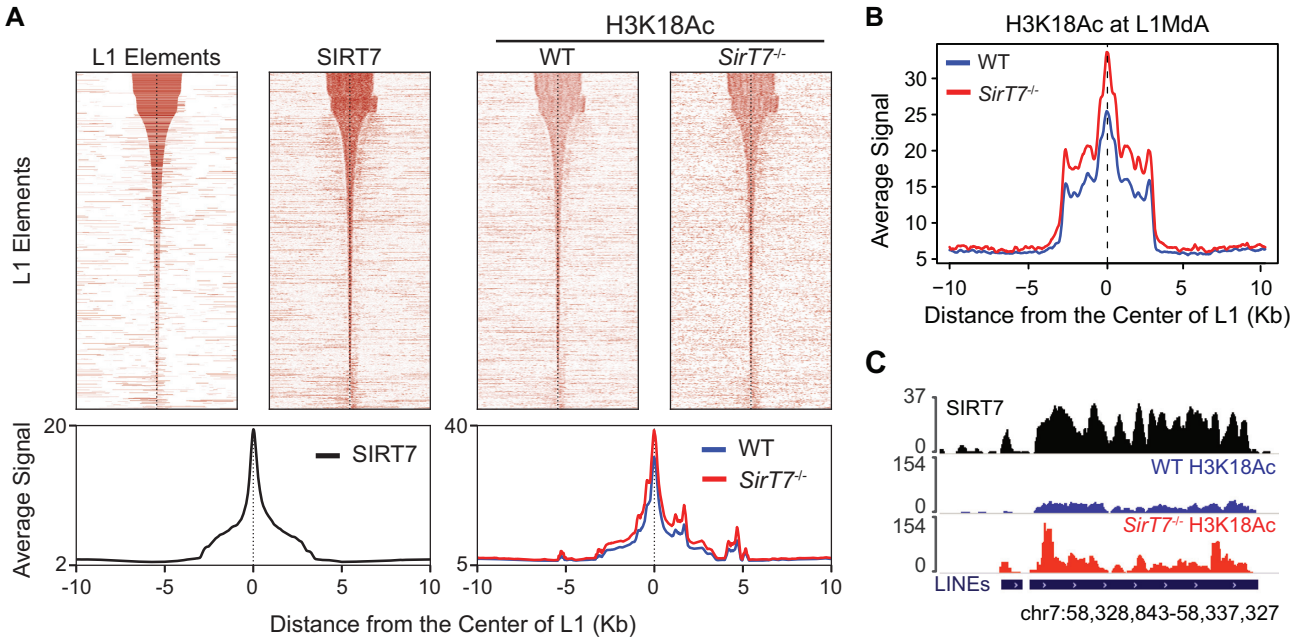

Figure 3. SIRT7 regulates H3K18Ac levels at L1 elements. (**A**, Top) Heat maps showing enrichment of SIRT7 and H3K18Ac in WT and *SirT7*$^{-/-}$ MEFs at genomic L1 elements. Left heat map (L1 elements) shows Smith–Waterman alignment score of genomic L1 elements as reported by RepeatMasker. (A, Bottom) Average enrichment profiles for (left) SIRT7 and (right) H3K18Ac in WT (blue) and *SirT7*$^{-/-}$ (red). (**B**) Average enrichment profiles for H3K18Ac in WT (blue) and *SirT7*$^{-/-}$ (red) in L1MdA family members. (**C**) Visualization of representative signal profiles for SIRT7 and H3K18Ac in WT and *SirT7*$^{-/-}$MEFs at an L1MdA locus.

Thus far, we employed standard RT-qPCR to quantify the effect of SIRT7 on L1 expression. According to a recent report (83), this approach could not distinguish authentic L1 transcripts (i.e. those transcribed from L1's own promoter) from L1 co-transcripts (i.e. those transcribed from a neighboring gene promoter). To determine whether SIRT7 regulates L1 expression from its own promoter, we devised a 5′RACE-qPCR strategy to specifically quantify full-length L1 transcripts in total cellular RNA (Supplementary Figure S7). Results were highly similar to those obtained with standard RT-qPCR (Supplementary Figure S8).

Overall, our results suggest that Lamin A/C is a downstream factor of H3K18 deacetylation but still crucial for L1 repression. In agreement with the common vision of the nuclear periphery as a heterochromatic compartment, and the known association of histone deacetylation with chromatin compaction (84), SIRT7 depletion was correlated with increased chromatin accessibility. Genomic DNA from *SirT7*$^{-/-}$ cells was more sensitive to Micrococcal Nuclease (MNase) treatment as compared with WT cells (Figure 6A), especially at L1 loci (Figure 6B).

To further determine the impact of SIRT7 in L1 repression, we questioned whether SIRT7 depletion increases L1 retrotransposition. To answer this question, WT and *SirT7*$^{-/-}$-derived cells were transfected with an L1-GFP retrotransposition reporter (85) (Figure 6C and Supplementary Figure S9). In this system, GFP expression only occurs after a successful retrotransposition event, which is measured by fluorescence-activated cell sorting (FACS). Importantly, SIRT7 deficiency resulted in a significant increase in the frequency of *de novo* retrotransposition events in SIRT7-depleted cells. We cannot rule out that the observed change in chromatin structure in *SirT7*$^{-/-}$ cells (Figure 6A) could affect the insertion site of the retrotransposition reporter. However, when analyzing the mean GFP fluorescence intensity in the GFP^{+} population (which corresponds to cells in which the construct has successfully retrotransposed) and in cells transfected with our GFP-based control vector we did not observe differences between WT and *SirT7*$^{-/-}$ cells (Supplementary Figure S9C and D, respectively), supporting our interpretation. This said, we cannot rule out either that the increased retrotransposition in *SirT7*$^{-/-}$ cells is solely the result of increased L1 expression. In addition, SIRT7 might modulate the retrotransposition lifecycle at other levels. Indeed, L1 elements require the host DNA repair machinery for integration (86) and we have previously published that SIRT7 regulates DNA repair (53).

Taken together, our results indicate that SIRT7 participates in L1 repression genome-wide in mouse and human cells. Mechanistically, our results support that SIRT7-mediated deacetylation of H3K18 is necessary for the recruitment of L1 to the nuclear periphery by their association with Lamin A/C to promote L1 transcriptional silencing and repress retrotransposition (Figure 6D).

DISCUSSION

Here we provide evidence supporting a new L1 transcriptional silencing mechanism that involves SIRT7 acting as a chromatin modifier and as a tethering factor of chromatin to the nuclear lamina. Sirtuins have multiple enzymatic activities including protein deacylation and mono-ADP ribosylation (87). Our results reveal that SIRT7-dependent

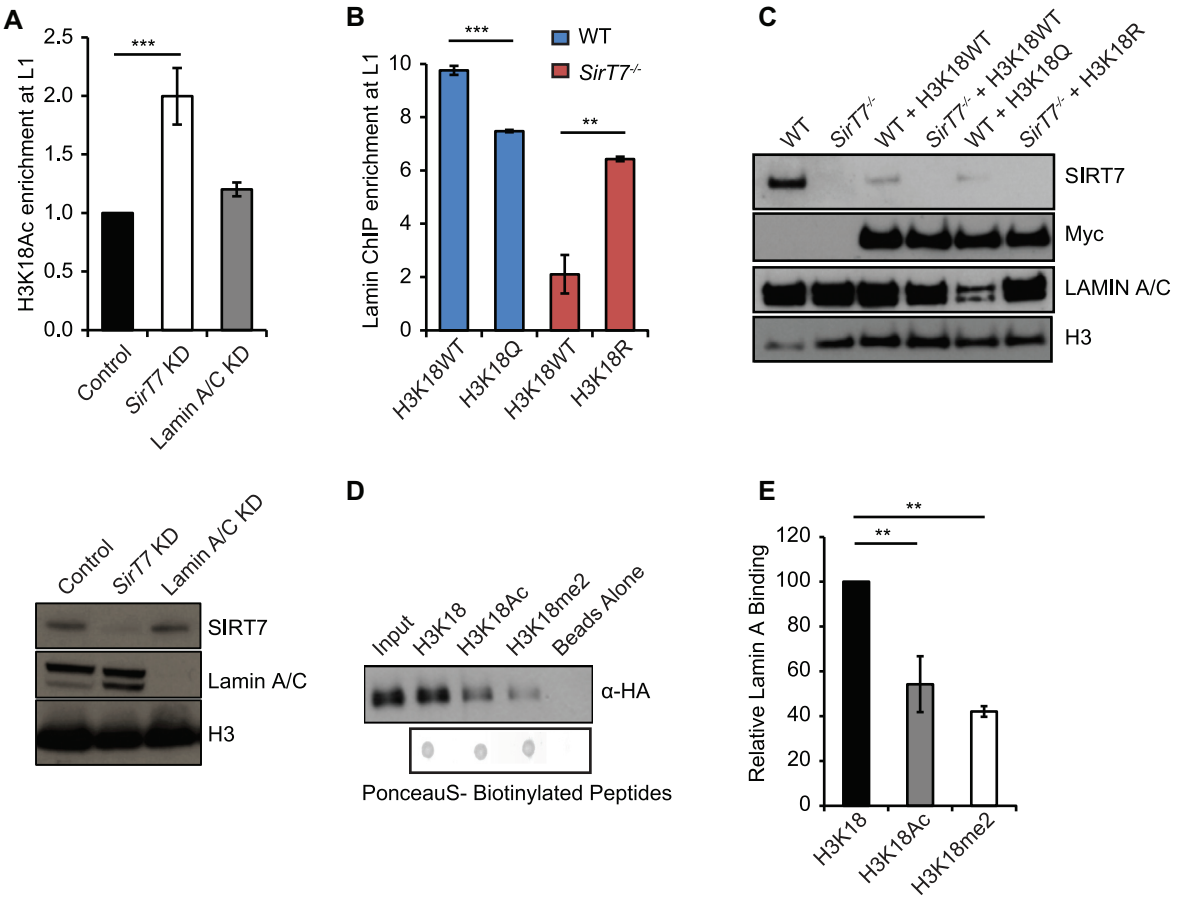

Figure 4. H3K18Ac modulates Lamin A/C levels at LINE-1 elements. (**A**) H3K18Ac ChIP-qPCR in HT1080 cells treated with siRNA Scramble (control), siRNA SirT7 (SirT7 KD) or Lamin A/C siRNA (Lamin A/C KD) using primers specific for human L1Hs consensus sequence and normalized to input DNA (Left). (Right) WB showing SirT7 and Lamin depletion. (**B**) Lamin ChIP in WT and *SirT7*$^{-/-}$ MEF cells overexpressing wild-type H3 (H3K18WT), and the histone mutants H3K18Q or H3K18R (acetylated, or deacetylated H3K18 residues, respectively). qPCR performed as in panel (A). (**C**) Western blot analysis of endogenous chromatin-bound SIRT7 and Lamin A/C from primary WT and *SirT7*$^{-/-}$ MEFs transduced with the indicated histone H3 vectors. Shown is anti-Myc as control for the ectopic expression of H3 vectors, and H3 for loading control. One representative blot is shown from two independent experiments. (**D** and **E**) Pull-down experiments using biotinylated peptides (H3, H3K18Ac and H3K18me2) incubated with purified Lamin A protein from HEK-293F cells transiently transfected with Lamin A HA-tagged. (D) Representative western blot analysis of pulled-down Lamin-HA (upper panel) and ponceau staining of the biotinylated peptides as loading control (bottom panel). Input represents 1% of the Lamin A HA-tagged loaded in the pulldowns. (E) Quantification by densitometry of the experiments in panel (D). The relative binding is expressed as fraction of Lamin A pulled-down normalized to the total biotinylated peptide used. Data represent mean ± SEM of three independent experiments per condition except otherwise indicated. $^{**}P < 0.01$; $^{***}P < 0.001$ by ANOVA single factor.

H3K18Ac deacetylation is a novel epigenetic mechanism for the suppression of L1 transcription in mouse embryonic fibroblasts and human cell lines. Studies looking at the breadth of human and mouse L1 variation though a phylogenetic lens have shown that L1 subfamilies can be distinguished by features in the promoter (5′UTR) region and grouped by evolutionary age (88,89). Upon deeper inspection of these characteristics, it becomes clear that new L1 subfamilies emerge from older, more repressed, subfamilies and quickly expand via retrotransposition before the cell can develop a working response. This classic evolutionary arms race has produced an array of cellular defenses against L1 tailored to the features unique to a particular L1 subfamily. Indeed, the epigenetic regulation of L1 expression in mammalian embryonic stem cells can vary among different L1 families: young L1 elements seem to be mostly silenced through SUV39h1/2-dependent H3K9me3 deposition (31), while more ancient ones are under KAP-1-mediated repression (34). Separate mechanisms might be also responsible for the suppression of evolutionary distinct L1s in more committed/differentiated cells. In support of this notion, our ChIP-seq analysis show that SIRT7 specifically binds the most recently evolved L1 families in both human and mouse cells (Figure 1D and Supplementary Figure S2B). SIRT7 is recruited to chromatin by its interaction with transcription factors (90). Despite SIRT7 associates with the entire L1 sequence, there is a peak of SIRT7 accumulation at the 5′UTR (Supplementary S1C). Therefore, it is possible that SIRT7 is recruited through a yet unknown partner at this specific site and it is then extended to the adjacent ORF.

Previous reports have already linked sirtuins enzymatic activities to the regulation of retrotransposon in fission yeast (91). In differentiated mammalian cells, only SIRT6 has been associated with L1 transcriptional repression (92).

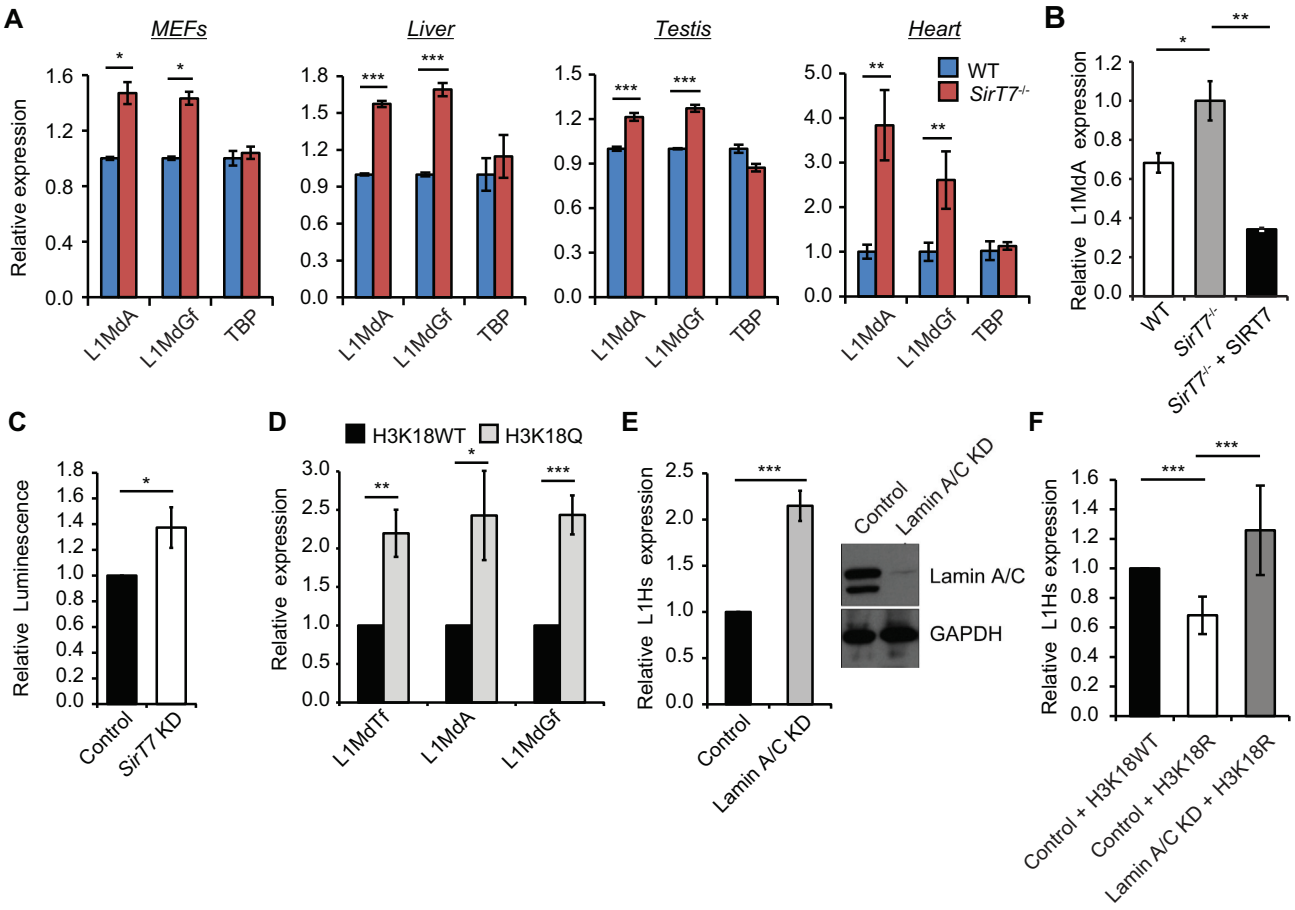

Figure 5. SIRT7 represses L1 expression through regulation of H3K18Ac levels. (**A** and **B**) mRNA expression of the indicated L1 families measured by qRT-PCR in MEFs and tissues from WT and *SirT7*$^{-/-}$ mice (A), and from SirT7$^{-/-}$derived MEFs overexpressing recombinant SIRT7 protein or empty vector (B). Data represent the mean ± SEM of three biological replicates. *P* values by ANOVA single Factor ($P < 0.05$; $^{**}P < 0.01$). (**C**) Luciferase activity of a 5'L1 UTR-FLuc reporter construct in HCT116_2C6.3 cells transfected with Scramble (Control) or SirT7 siRNA (SirT7 KD). Data represent the mean luminescence normalized by cell viability ± SEM of four independent transfection replicates. (**D**) qRT-PCR of the indicated L1 families from WT MEFs overexpressing wild-type histone H3 (H3K18WT) and the histone mutant H3K18Q (acetylated H3K18 residue). (**E**) qRT-PCR expression of L1Hs transcripts in HT1080 cells transduced with Scramble (Control) or Lamin A/C siRNA (Lamin A/C KD). WB showing Lamin depletion (right). (**F**) qRT-PCR of L1Hs transcripts in HT1080 cells overexpressing wild-type histone H3 (H3K18WT) and the histone mutant H3K18R (deacetylated H3K18 residue) and transduced with Scramble (Control) or Lamin A/C siRNA (Lamin A/C KD) as indicated. (D and F) Data represent the mean ± SEM of $N \geq 3$ independent experiments. *P* values by paired *T*-test ($^{*}P < 0.05$; $^{**}P < 0.01$; $^{***}P < 0.001$).

Mechanistically, SIRT6 is able to bind L1 where it mono-ADP-ribosylates KAP-1, facilitating the formation of the KAP-1/HP-1α corepressor complex at L1, which has been linked to the regulation of middle-aged subfamilies of L1 (34). Despite that SIRT6 has been shown to deacetylase H3K18Ac in pericentric heterochromatin, loss of SIRT6 did not change H3K18Ac levels at L1 (93) suggesting that SIRT6 and SIRT7 have developed different mechanisms to mediate L1 transcriptional repression. It is tempting to speculate that SIRT6 and SIRT7 are specialized in the regulation of different L1 families according to their evolutionary age. Future work will be required to examine SIRT6 and SIRT7 occupancy at L1 loci in different cellular context to determine the level of redundancy of these sirtuins in the repression of L1s. Nevertheless, our results expand the role of sirtuins in the repression of mobile elements, and strongly support histone acetylation as an important player in L1 transcriptional regulation.

H3K18Ac has been previously linked to transcriptional regulation (76,77,93). How H3K18Ac levels mechanistically contribute to regulate transcription is only understood in the case of pericentric chromatin, in which SIRT6-dependent H3K18 deacetylation stabilizes the transcriptional repressor KAP1 (93). Our results suggest that H3K18 deacetylation is required for the tethering of L1s to the nuclear periphery by their association with Lamin A/C (Figure 4), expanding the molecular mechanism of action of this histone modification. Consistently, ChIP-seq analyses based on our and previous reports (44) indicate L1 association with LADs is restricted to SIRT7-bound young L1 families, which are still capable of transcription (Figure 1D and Supplementary Figure S2B). In addition, we show that depletion of Lamin A/C results in transcriptional upregulation of these L1 subfamilies (Figure 5E), and that H3K18 deacetylation is not sufficient to repress L1 expression in the absence of Lamin A/C (Figure 5F). These results strongly support that L1-Lamin A/C association is necessary for L1

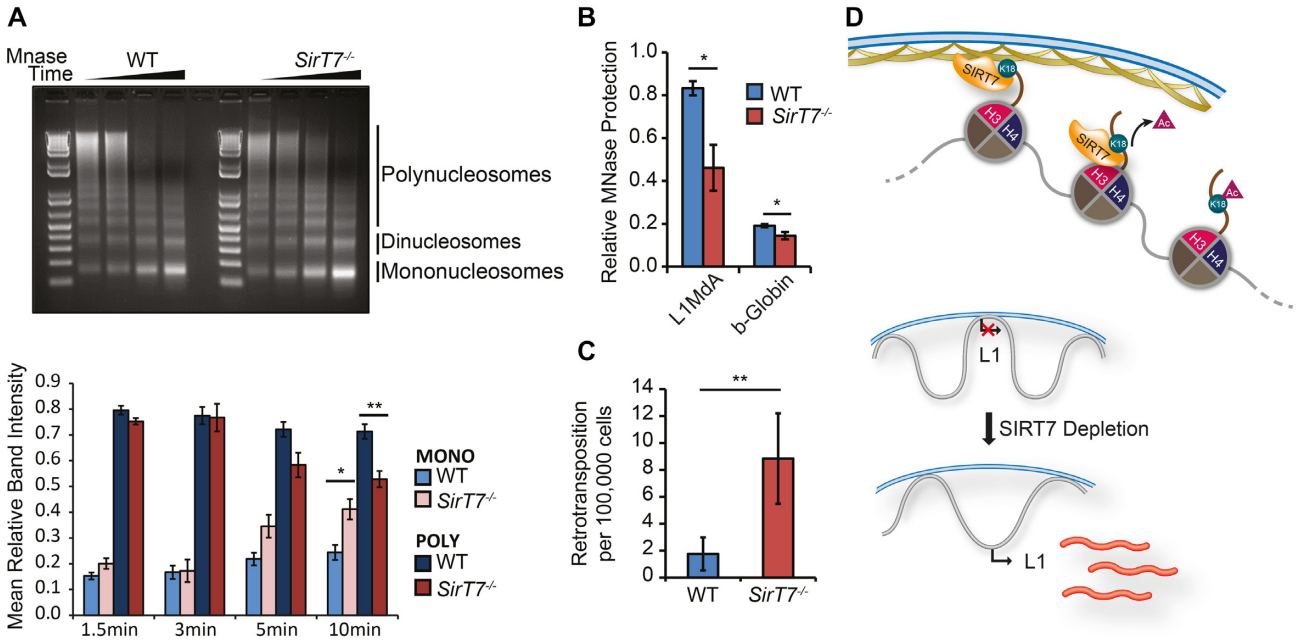

Figure 6. Increase L1 retrotransposition in the absence of SIRT7. (**A** and **B**) Chromatin accessibility assay in WT and *SirT7*$^{-/-}$cells. (A) Isolated nuclei from WT and SIRT7 KO cells were digested with 4 units of micrococcal nuclease (MNase) for 1.5, 3, 5 and 10 min. Different nucleosomal fractions (mono, di and polynucleosomes) were separated by gel electrophoresis. (Top) Representative western blot. (Bottom) Band density quantification using ImageJ software. Results are expressed as the mean ± SEM of three independent experiments. *$P < 0.05$; **$P < 0.01$ by ANOVA single factor. (**B**) qPCR showing protection of MNase-digested DNA at the 5 min time point relative to non-treated DNA at indicated loci in WT and *SirT7*$^{-/-}$cells. Primers were designed to target the promoters of the L1MdA consensus sequence and the β-globin gene to obtain PCR amplicons longer than the length of a single nucleosome. Reduced amplification indicates more MNase digestion, which is interpreted as the presence of more accessible chromatin at the assayed loci. Data represent mean ± SEM of three independent experiments per condition after normalization to actin gene expression. *$P < 0.05$; **$P < 0.01$ by ANOVA single factor. (**C**) FACS analysis showing number of GFP^{+} events per 10^5 cells in WT and *SirT7*$^{-/-}$ MEFs. Quantification (mean ± SEM of 4 samples/genotype. *$P = 0.047$ by one tail Student's *t*-test). (**D**) Mechanistic model: (Top) SIRT7 is found at L1 loci, where it deacetylates H3K18Ac. Lamin A binds SIRT7 and to deacetylated H3K18 L1 chromatin. (Bottom) In this way, SIRT7 promotes the recruitment of L1 elements to the nuclear periphery resulting in the generation of a repressive chromatin environment that prevents L1 expression. Upon SIRT7 depletion, L1 elements are relocated toward the nuclear interior concomitantly to their activation.

repression, which is in agreement with the common vision of the nuclear lamina as a transcriptional repressive environment and a major player for heterochromatin maintenance (46).

Mechanistically, Lamin A/C promotes the anchoring of heterochromatin to the nuclear periphery (94,95,96). The mechanisms by which Lamin A/C tethers heterochromatin to the nuclear rim are just starting to be revealed, for review see (97). Lamin A/C is able to bind DNA (98), core histones (80) and several inner nuclear membrane proteins (99). However, the effects of histone post-translational modifications in Lamin A/C binding to chromatin are largely unknown. LADs are enriched in histone marks that are associated with transcriptional repression such as H3K9me3 and H3K27me3 (97). Depletion of the methyltransferases responsible for these histones marks results in reduced heterochromatin at the nuclear periphery (100). However, the methylation status of these histone marks does not affect Lamin A interaction with the histone H3 tail (101). Histone deacetylation is also important for gene positioning at the nuclear periphery and gene repression (51,84,102,103). The underlying molecular players are largely unknown and it has mainly been attributed to HDAC3 activity. Cells lacking HDAC3 have a significant decrease in the amount of heterochromatin, especially at the periphery (104). HDAC3 is recruited to the nuclear lamina via its interaction with inner nuclear transmembrane proteins such as LAP2β (105) and emerin (106), along with specific transcription factors such as cKROX (51). However, whether histone acetylation status favors the interaction of Lamin A/C to chromatin has not directly been tested. We propose that the acetylation state at H3K18, which is regulated at L1s by SIRT7, promotes the affinity of chromatin to Lamin A/C. Indeed, we show that Lamin A/C specifically interact with unmodified histone H3, whereas acetylation on H3K18 disrupts this interaction (Figure 4D and E). We cannot rule out that L1 tethering to the nuclear periphery can be mediated by SIRT7 interaction with nuclear membrane proteins or other bridge factors. In this regard, our results indicate that Lamin A/C and SIRT7 proteins can directly interact (Figure 2B and Supplementary Figure S3), and suggest that this interaction could cooperate with SIRT7-mediated H3K18 deacetylation to position L1s at the nuclear periphery. Indeed, the interplay between the nuclear lamina and Sirtuins has been previously observed. SIRT1 is recruited to the nuclear envelope through direct interaction with Lamin A, which in turn activates SIRT1 deacetylase activity toward substrates such as p53 (79). Similarly, SIRT6 deacetylase activity is enhanced upon SIRT6–Lamin A interaction, which regulates SIRT6 recruitment to chromatin upon DNA damage (78). However, whether this association occurs at chromatin regions located at the nuclear periphery is unknown.

In our model, the presence of Lamin A/C does not impact SIRT7 deacetylase activity as the levels of H3K18Ac at L1 loci do not change upon Lamin A/C knockdown (Figure 4A). However, we do not know if, alternatively, Lamin A/C could be a substrate for SIRT7 enzymatic activity. In this regard, total chromatin levels of Lamin A/C are similar in WT and *SirT7*$^{-/-}$ MEFs (Figure 2D). Future work will be required to fully understand the molecular interplay between SIRT7 and Lamin A/C in the regulation of L1 expression.

On top of its role in transcriptional regulation, Lamin is essential to maintain nuclear organization (107). The anchoring of specific chromatin domains to the nuclear lamina was one of the first mechanistic explanations for how nuclear architecture is established and maintained (42). Lamin-mediated regulatory mechanisms become most relevant considering its disruption in cancer and aging cells (108,109,110). Diseases associated with Lamin mutations, such as progeria, provide evidence that Lamin depletion causes large scale reorganization of LAD chromatin structure, including regions of H3K4me3 and H3K27me3 marks (111). We provide several lines of evidence supporting that L1 association with the nuclear lamina becomes disrupted upon SIRT7 depletion. Considering the abundance of these elements in the mammalian genome (1,2), disruption of the anchoring of L1 to Lamin A/C might impact the localization to or away from the nuclear periphery of adjacent chromatin domains inducing large-scale chromatin organization changes. Interestingly, recent evidence has linked H3K18Ac with early chromatin conformation events (112). The authors found H3K18Ac at chromatin nucleation sites, which dictate the emergence of chromatin architecture that occurs at the onset of transcription activation in the zygote. It is known that in this window of time L1 gets reactivated (113). It is possible that L1 activation is a consequence of the early chromatin conformation events and/or, as recently suggested (114), necessary for these events to occur. Nevertheless, inherent in our findings is that the loss of Lamin A/C observed in aging and cancer cells will reduce the capacity for SIRT7 to anchor L1 elements to nuclear lamina, promote L1 activation and its associated phenotypes such as increased DNA damage and altered gene expression profiles.

Recent reports demonstrated that activation of endogenous L1 elements evolves progressively during cell senescence resulting in the activation of sterile inflammation (115,116). These reports mechanistically establish L1 transcriptional dysregulation as a plausible component of the type I interferon response activation and the senescence-associated secretory phenotype and therefore, with the process of aging. We previously provided evidence of an accelerated aging phenotype and compromised genome integrity in the SIRT7 knockout mouse, which was in part due to impaired DNA damage repair (53). In this report we unveiled a novel interplay between SIRT7-mediated chromatin regulation, Lamin A/C and repression of L1 elements, which adds to the molecular mechanisms of SIRT7-mediated genome regulation. Taken together, our findings further establish SIRT7 as safeguard of genome integrity and a potential therapeutic target to ameliorate age-related pathologies.

DATA AVAILABILITY

ChIP-sequence data used in this study is available at GEO Accession Number GSE106964.

Lamin B1 DamID performed in MEFs was obtained from GEO Series GSE36132. Called peaks for ChIP of H3K27Ac, H3K4me1, H3K4me3 and POLR2A were obtained from the ENCODE project under accession numbers ENCSR000CDI, ENCSR000CAZ, ENCSR000CBA and ENCSR000CBX.

SUPPLEMENTARY DATA

Supplementary Data are available at NAR Online.

FUNDING

Human Genetics Institute of New Jersey (HGINJ) (to L.S.); Spanish Ministry of Education, Culture, and Sports [EX-2010-278 to B.N.V.]; HGINJ; FPI fellowship [BES-2012-052200 to N.G.S.]; The Spanish Ministry of Economy and Competitiveness (MINECO) [SAF2014-55964-R, SAF2017-88975-R to A.V.]; La Marató de TV3, Spain; National Institute of General Medical Sciences (NIGMS) Grant [P50GM107632 to W.A.]. Funding for open access charge: Internal Institute grant.

Conflict of interest statement. None declared.

REFERENCES

1. Lander,E.S., Linton,L.M., Birren,B., Nusbaum,C., Zody,M.C., Baldwin,J., Devon,K., Dewar,K., Doyle,M., FitzHugh,W. *et al.* (2001) Initial sequencing and analysis of the human genome. *Nature*, **409**, 860–921.
2. Waterston,R.H., Lindblad-Toh,K., Birney,E., Rogers,J., Abril,J.F., Agarwal,P., Agarwala,R., Ainscough,R., Alexandersson,M., An,P. *et al.* (2002) Initial sequencing and comparative analysis of the mouse genome. *Nature*, **420**, 520–562.
3. Kazazian,H.H. Jr. (2004) Mobile elements: drivers of genome evolution. *Science*, **303**, 1626–1632.
4. Branciforte,D. and Martin,S.L. (1994) Developmental and cell type specificity of LINE-1 expression in mouse testis: implications for transposition. *Mol. Cell Biol.*, **14**, 2584–2592.
5. Trelogan,S.A. and Martin,S.L. (1995) Tightly regulated, developmentally specific expression of the first open reading frame from LINE-1 during mouse embryogenesis. *Proc. Natl. Acad. Sci. U.S.A.*, **92**, 1520–1524.
6. Ergun,S., Buschmann,C., Heukeshoven,J., Dammann,K., Schnieders,F., Lauke,H., Chalajour,F., Kilic,N., Stratling,W.H. and Schumann,G.G. (2004) Cell type-specific expression of LINE-1 open reading frames 1 and 2 in fetal and adult human tissues. *J. Biol. Chem.*, **279**, 27753–27763.
7. Rosser,J.M. and An,W. (2012) L1 expression and regulation in humans and rodents. *Front. Biosci.*, **4**, 2203–2225.
8. Baillie,J.K., Barnett,M.W., Upton,K.R., Gerhardt,D.J., Richmond,T.A., De Sapio,F., Brennan,P.M., Rizzu,P., Smith,S., Fell,M. *et al.* (2011) Somatic retrotransposition alters the genetic landscape of the human brain. *Nature*, **479**, 534–537.
9. Muotri,A.R., Chu,V.T., Marchetto,M.C., Deng,W., Moran,J.V. and Gage,F.H. (2005) Somatic mosaicism in neuronal precursor cells mediated by L1 retrotransposition. *Nature*, **435**, 903–910.
10. Coufal,N.G., Garcia-Perez,J.L., Peng,G.E., Yeo,G.W., Mu,Y., Lovci,M.T., Morell,M., O'Shea,K.S., Moran,J.V. and Gage,F.H. (2009) L1 retrotransposition in human neural progenitor cells. *Nature*, **460**, 1127–1131.
11. Evrony,G.D., Cai,X., Lee,E., Hills,L.B., Elhosary,P.C., Lehmann,H.S., Parker,J.J., Atabay,K.D., Gilmore,E.C., Poduri,A. *et al.* (2012) Single-neuron sequencing analysis of L1

retrotransposition and somatic mutation in the human brain. *Cell*, **151**, 483–496.
12. Faulkner,G.J., Kimura,Y., Daub,C.O., Wani,S., Plessy,C., Irvine,K.M., Schroder,K., Cloonan,N., Steptoe,A.L., Lassmann,T. *et al.* (2009) The regulated retrotransposon transcriptome of mammalian cells. *Nat. Genet.*, **41**, 563–571.
13. Han,J.S., Szak,S.T. and Boeke,J.D. (2004) Transcriptional disruption by the L1 retrotransposon and implications for mammalian transcriptomes. *Nature*, **429**, 268–274.
14. Ohms,S. and Rangasamy,D. (2014) Silencing of LINE-1 retrotransposons contributes to variation in small noncoding RNA expression in human cancer cells. *Oncotarget*, **5**, 4103–4117.
15. Goodier,J.L., Ostertag,E.M. and Kazazian,H.H. Jr. (2000) Transduction of 3′-flanking sequences is common in L1 retrotransposition. *Hum. Mol. Genet.*, **9**, 653–657.
16. Pickeral,O.K., Makalowski,W., Boguski,M.S. and Boeke,J.D. (2000) Frequent human genomic DNA transduction driven by LINE-1 retrotransposition. *Genome Res.*, **10**, 411–415.
17. Dewannieux,M., Esnault,C. and Heidmann,T. (2003) LINE-mediated retrotransposition of marked Alu sequences. *Nat. Genet.*, **35**, 41–48.
18. Dewannieux,M. and Heidmann,T. (2005) L1-mediated retrotransposition of murine B1 and B2 SINEs recapitulated in cultured cells. *J. Mol. Biol.*, **349**, 241–247.
19. Gasior,S.L., Wakeman,T.P., Xu,B. and Deininger,P.L. (2006) The human LINE-1 retrotransposon creates DNA double-strand breaks. *J. Mol. Biol.*, **357**, 1383–1393.
20. Wallace,N.A., Belancio,V.P. and Deininger,P.L. (2008) L1 mobile element expression causes multiple types of toxicity. *Gene*, **419**, 75–81.
21. Belgnaoui,S.M., Gosden,R.G., Semmes,O.J. and Haoudi,A. (2006) Human LINE-1 retrotransposon induces DNA damage and apoptosis in cancer cells. *Cancer Cell Int*, **6**, 13.
22. Belancio,V.P., Roy-Engel,A.M., Pochampally,R.R. and Deininger,P. (2010) Somatic expression of LINE-1 elements in human tissues. *Nucleic Acids Res.*, **38**, 3909–3922.
23. De Cecco,M., Criscione,S.W., Peterson,A.L., Neretti,N., Sedivy,J.M. and Kreiling,J.A. (2013) Transposable elements become active and mobile in the genomes of aging mammalian somatic tissues. *Aging (Albany NY)*, **5**, 867–883.
24. Rodic,N. and Burns,K.H. (2013) Long interspersed element-1 (LINE-1): passenger or driver in human neoplasms? *PLos Genet.*, **9**, e1003402.
25. Scott,E.C., Gardner,E.J., Masood,A., Chuang,N.T., Vertino,P.M. and Devine,S.E. (2016) A hot L1 retrotransposon evades somatic repression and initiates human colorectal cancer. *Genome Res.*, **26**, 745–755.
26. Shukla,R., Upton,K.R., Munoz-Lopez,M., Gerhardt,D.J., Fisher,M.E., Nguyen,T., Brennan,P.M., Baillie,J.K., Collino,A., Ghisletti,S. *et al.* (2013) Endogenous retrotransposition activates oncogenic pathways in hepatocellular carcinoma. *Cell*, **153**, 101–111.
27. Miki,Y., Nishisho,I., Horii,A., Miyoshi,Y., Utsunomiya,J., Kinzler,K.W., Vogelstein,B. and Nakamura,Y. (1992) Disruption of the APC gene by a retrotransposal insertion of L1 sequence in a colon cancer. *Cancer Res.*, **52**, 643–645.
28. Goodier,J.L. (2016) Restricting retrotransposons: a review. *Mob. DNA*, **7**, 16.
29. Lee,H.J., Hore,T.A. and Reik,W. (2014) Reprogramming the methylome: erasing memory and creating diversity. *Cell Stem Cell*, **14**, 710–719.
30. Pezic,D., Manakov,S.A., Sachidanandam,R. and Aravin,A.A. (2014) piRNA pathway targets active LINE1 elements to establish the repressive H3K9me3 mark in germ cells. *Genes Dev.*, **28**, 1410–1428.
31. Bulut-Karslioglu,A., De La Rosa-Velazquez,I.A., Ramirez,F., Barenboim,M., Onishi-Seebacher,M., Arand,J., Galan,C., Winter,G.E., Engist,B., Gerle,B. *et al.* (2014) Suv39h-dependent H3K9me3 marks intact retrotransposons and silences LINE elements in mouse embryonic stem cells. *Mol. Cell*, **55**, 277–290.
32. Arand,J., Spieler,D., Karius,T., Branco,M.R., Meilinger,D., Meissner,A., Jenuwein,T., Xu,G., Leonhardt,H., Wolf,V. *et al.* (2012) In vivo control of CpG and non-CpG DNA methylation by DNA methyltransferases. *PLos Genet.*, **8**, e1002750.
33. Aravin,A.A., Sachidanandam,R., Bourc'his,D., Schaefer,C., Pezic,D., Toth,K.F., Bestor,T. and Hannon,G.J. (2008) A piRNA pathway primed by individual transposons is linked to de novo DNA methylation in mice. *Mol. Cell*, **31**, 785–799.
34. Castro-Diaz,N., Ecco,G., Coluccio,A., Kapopoulou,A., Yazdanpanah,B., Friedli,M., Duc,J., Jang,S.M., Turelli,P. and Trono,D. (2014) Evolutionally dynamic L1 regulation in embryonic stem cells. *Genes Dev.*, **28**, 1397–1409.
35. Day,D.S., Luquette,L.J., Park,P.J. and Kharchenko,P.V. (2010) Estimating enrichment of repetitive elements from high-throughput sequence data. *Genome Biol.*, **11**, R69.
36. Kannan,M., Li,J., Fritz,S.E., Husarek,K.E., Sanford,J.C., Sullivan,T.L., Tiwary,P.K., An,W., Boeke,J.D. and Symer,D.E. (2017) Dynamic silencing of somatic L1 retrotransposon insertions reflects the developmental and cellular contexts of their genomic integration. *Mob. DNA*, **8**, 8.
37. Garcia-Perez,J.L., Morell,M., Scheys,J.O., Kulpa,D.A., Morell,S., Carter,C.C., Hammer,G.D., Collins,K.L., O'Shea,K.S., Menendez,P. *et al.* (2010) Epigenetic silencing of engineered L1 retrotransposition events in human embryonic carcinoma cells. *Nature*, **466**, 769–773.
38. Pal,S. and Tyler,J.K. (2016) Epigenetics and aging. *Sci. Adv.*, **2**, e1600584.
39. Lopez-Otin,C., Blasco,M.A., Partridge,L., Serrano,M. and Kroemer,G. (2013) The hallmarks of aging. *Cell*, **153**, 1194–1217.
40. Brunet,A. and Berger,S.L. (2014) Epigenetics of aging and aging-related disease. *J. Gerontol. A Biol. Sci. Med. Sci.*, **69**(Suppl. 1), S17–S20.
41. Baylin,S.B. and Jones,P.A. (2016) Epigenetic determinants of cancer. *Cold Spring Harb.Perspect. Biol.*, **8**, a019505.
42. Guelen,L., Pagie,L., Brasset,E., Meuleman,W., Faza,M.B., Talhout,W., Eussen,B.H., de Klein,A., Wessels,L., de Laat,W. *et al.* (2008) Domain organization of human chromosomes revealed by mapping of nuclear lamina interactions. *Nature*, **453**, 948–951.
43. Peric-Hupkes,D., Meuleman,W., Pagie,L., Bruggeman,S.W., Solovei,I., Brugman,W., Graf,S., Flicek,P., Kerkhoven,R.M., van Lohuizen,M. *et al.* (2010) Molecular maps of the reorganization of genome-nuclear lamina interactions during differentiation. *Mol. Cell*, **38**, 603–613.
44. Meuleman,W., Peric-Hupkes,D., Kind,J., Beaudry,J.B., Pagie,L., Kellis,M., Reinders,M., Wessels,L. and van Steensel,B. (2013) Constitutive nuclear lamina-genome interactions are highly conserved and associated with A/T-rich sequence. *Genome Res.*, **23**, 270–280.
45. Kind,J., Pagie,L., de Vries,S.S., Nahidiazar,L., Dey,S.S., Bienko,M., Zhan,Y., Lajoie,B., de Graaf,C.A., Amendola,M. *et al.* (2015) Genome-wide maps of nuclear lamina interactions in single human cells. *Cell*, **163**, 134–147.
46. van Steensel,B. and Belmont,A.S. (2017) Lamina-associated domains: links with chromosome architecture, heterochromatin, and gene repression. *Cell*, **169**, 780–791.
47. Tumbar,T., Sudlow,G. and Belmont,A.S. (1999) Large-scale chromatin unfolding and remodeling induced by VP16 acidic activation domain. *J. Cell Biol.*, **145**, 1341–1354.
48. Tumbar,T. and Belmont,A.S. (2001) Interphase movements of a DNA chromosome region modulated by VP16 transcriptional activator. *Nat. Cell Biol.*, **3**, 134–139.
49. Finlan,L.E., Sproul,D., Thomson,I., Boyle,S., Kerr,E., Perry,P., Ylstra,B., Chubb,J.R. and Bickmore,W.A. (2008) Recruitment to the nuclear periphery can alter expression of genes in human cells. *PLos Genet.*, **4**, e1000039.
50. Reddy,K.L., Zullo,J.M., Bertolino,E. and Singh,H. (2008) Transcriptional repression mediated by repositioning of genes to the nuclear lamina. *Nature*, **452**, 243–247.
51. Zullo,J.M., Demarco,I.A., Pique-Regi,R., Gaffney,D.J., Epstein,C.B., Spooner,C.J., Luperchio,T.R., Bernstein,B.E., Pritchard,J.K., Reddy,K.L. *et al.* (2012) DNA sequence-dependent compartmentalization and silencing of chromatin at the nuclear lamina. *Cell*, **149**, 1474–1487.
52. David G Brownstein,R.b. (2003) Manipulating the mouse embryo: a laboratory manual. third edition. by andras nagy, marina gertsenstein, kristina vintersten, and richard behringer. *Q. Rev. Biol.*, **78**, 365–365.

53. Vazquez,B.N., Thackray,J.K., Simonet,N.G., Kane-Goldsmith,N., Martinez-Redondo,P., Nguyen,T., Bunting,S., Vaquero,A., Tischfield,J.A. and Serrano,L. (2016) SIRT7 promotes genome integrity and modulates non-homologous end joining DNA repair. *EMBO J.*, **35**, 1483–1595.
54. Serrano,L., Martinez-Redondo,P., Marazuela-Duque,A., Vazquez,B.N., Dooley,S.J., Voigt,P., Beck,D.B., Kane-Goldsmith,N., Tong,Q., Rabanal,R.M. *et al.* (2013) The tumor suppressor SirT2 regulates cell cycle progression and genome stability by modulating the mitotic deposition of H4K20 methylation. *Genes Dev.*, **27**, 639–653.
55. Han,J.S. and Boeke,J.D. (2004) A highly active synthetic mammalian retrotransposon. *Nature*, **429**, 314–318.
56. Bosch-Presegue,L., Raurell-Vila,H., Thackray,J.K., Gonzalez,J., Casal,C., Kane-Goldsmith,N., Vizoso,M., Brown,J.P., Gomez,A., Ausio,J. *et al.* (2017) Mammalian HP1 isoforms have specific roles in heterochromatin structure and organization. *Cell Rep.*, **21**, 2048–2057.
57. Bolger,A.M., Lohse,M. and Usadel,B. (2014) Trimmomatic: a flexible trimmer for Illumina sequence data. *Bioinformatics*, **30**, 2114–2120.
58. Langmead,B., Trapnell,C., Pop,M. and Salzberg,S.L. (2009) Ultrafast and memory-efficient alignment of short DNA sequences to the human genome. *Genome Biol.*, **10**, R25.
59. Li,H., Handsaker,B., Wysoker,A., Fennell,T., Ruan,J., Homer,N., Marth,G., Abecasis,G. and Durbin,R. (2009) The Sequence Alignment/Map format and SAMtools. *Bioinformatics*, **25**, 2078–2079.
60. Zhang,Y., Liu,T., Meyer,C.A., Eeckhoute,J., Johnson,D.S., Bernstein,B.E., Nusbaum,C., Myers,R.M., Brown,M., Li,W. *et al.* (2008) Model-based analysis of ChIP-Seq (MACS). *Genome Biol.*, **9**, R137.
61. Ramirez,F., Ryan,D.P., Gruning,B., Bhardwaj,V., Kilpert,F., Richter,A.S., Heyne,S., Dundar,F. and Manke,T. (2016) deepTools2: a next generation web server for deep-sequencing data analysis. *Nucleic Acids Res.*, **44**, W160–W165.
62. Quinlan,A.R. and Hall,I.M. (2010) BEDTools: a flexible suite of utilities for comparing genomic features. *Bioinformatics*, **26**, 841–842.
63. Shin,H., Liu,T., Manrai,A.K. and Liu,X.S. (2009) CEAS: cis-regulatory element annotation system. *Bioinformatics*, **25**, 2605–2606.
64. Dale,R.K., Matzat,L.H. and Lei,E.P. (2014) metaseq: a Python package for integrative genome-wide analysis reveals relationships between chromatin insulators and associated nuclear mRNA. *Nucleic Acids Res.*, **42**, 9158–9170.
65. Dale,R.K., Pedersen,B.S. and Quinlan,A.R. (2011) Pybedtools: a flexible Python library for manipulating genomic datasets and annotations. *Bioinformatics*, **27**, 3423–3424.
66. Thorvaldsdottir,H., Robinson,J.T. and Mesirov,J.P. (2013) Integrative Genomics Viewer (IGV): high-performance genomics data visualization and exploration. *Brief. Bioinform.*, **14**, 178–192.
67. Siepel,A., Bejerano,G., Pedersen,J.S., Hinrichs,A.S., Hou,M., Rosenbloom,K., Clawson,H., Spieth,J., Hillier,L.W., Richards,S. *et al.* (2005) Evolutionarily conserved elements in vertebrate, insect, worm, and yeast genomes. *Genome Res.*, **15**, 1034–1050.
68. Siepel,A. and Haussler,D. (2004) Combining phylogenetic and hidden Markov models in biosequence analysis. *J. Comput. Biol.*, **11**, 413–428.
69. McLean,C.Y., Bristor,D., Hiller,M., Clarke,S.L., Schaar,B.T., Lowe,C.B., Wenger,A.M. and Bejerano,G. (2010) GREAT improves functional interpretation of cis-regulatory regions. *Nat. Biotechnol.*, **28**, 495–501.
70. Jurka,J. (2000) Repbase update: a database and an electronic journal of repetitive elements. *Trends Genet.*, **16**, 418–420.
71. Jurka,J., Kapitonov,V.V., Pavlicek,A., Klonowski,P., Kohany,O. and Walichiewicz,J. (2005) Repbase Update, a database of eukaryotic repetitive elements. *Cytogenet. Genome Res.*, **110**, 462–467.
72. Mates,L. (2011) Rodent transgenesis mediated by a novel hyperactive Sleeping Beauty transposon system. *Methods Mol. Biol.*, **738**, 87–99.
73. Ostertag,E.M., Prak,E.T., DeBerardinis,R.J., Moran,J.V. and Kazazian,H.H. Jr. (2000) Determination of L1 retrotransposition kinetics in cultured cells. *Nucleic Acids Res.*, **28**, 1418–1423.
74. Ford,E., Voit,R., Liszt,G., Magin,C., Grummt,I. and Guarente,L. (2006) Mammalian Sir2 homolog SIRT7 is an activator of RNA polymerase I transcription. *Genes Dev.*, **20**, 1075–1080.
75. Wang,Z., Zang,C., Rosenfeld,J.A., Schones,D.E., Barski,A., Cuddapah,S., Cui,K., Roh,T.Y., Peng,W., Zhang,M.Q. *et al.* (2008) Combinatorial patterns of histone acetylations and methylations in the human genome. *Nat. Genet.*, **40**, 897–903.
76. Barber,M.F., Michishita-Kioi,E., Xi,Y., Tasselli,L., Kioi,M., Moqtaderi,Z., Tennen,R.I., Paredes,S., Young,N.L., Chen,K. *et al.* (2012) SIRT7 links H3K18 deacetylation to maintenance of oncogenic transformation. *Nature*, **487**, 114–118.
77. Shin,J., He,M., Liu,Y., Paredes,S., Villanova,L., Brown,K., Qiu,X., Nabavi,N., Mohrin,M., Wojnoonski,K. *et al.* (2013) SIRT7 represses Myc activity to suppress ER stress and prevent fatty liver disease. *Cell Rep.*, **5**, 654–665.
78. Ghosh,S., Liu,B., Wang,Y., Hao,Q. and Zhou,Z. (2015) Lamin a is an endogenous SIRT6 activator and promotes SIRT6-Mediated DNA repair. *Cell Rep.*, **13**, 1396–1406.
79. Liu,B., Ghosh,S., Yang,X., Zheng,H., Liu,X., Wang,Z., Jin,G., Zheng,B., Kennedy,B.K., Suh,Y. *et al.* (2012) Resveratrol rescues SIRT1-dependent adult stem cell decline and alleviates progeroid features in laminopathy-based progeria. *Cell Metab.*, **16**, 738–750.
80. Taniura,H., Glass,C. and Gerace,L. (1995) A chromatin binding site in the tail domain of nuclear lamins that interacts with core histones. *J. Cell Biol.*, **131**, 33–44.
81. Vakhrusheva,O., Braeuer,D., Liu,Z., Braun,T. and Bober,E. (2008) Sirt7-dependent inhibition of cell growth and proliferation might be instrumental to mediate tissue integrity during aging. *J. Physiol. Pharmacol.*, **59**(Suppl. 9), 201–212.
82. Yoshizawa,T., Karim,M.F., Sato,Y., Senokuchi,T., Miyata,K., Fukuda,T., Go,C., Tasaki,M., Uchimura,K., Kadomatsu,T. *et al.* (2014) SIRT7 controls hepatic lipid metabolism by regulating the ubiquitin-proteasome pathway. *Cell Metab.*, **19**, 712–721.
83. Deininger,P., Morales,M.E., White,T.B., Baddoo,M., Hedges,D.J., Servant,G., Srivastav,S., Smither,M.E., Concha,M., DeHaro,D.L. *et al.* (2017) A comprehensive approach to expression of L1 loci. *Nucleic Acids Res.*, **45**, e31.
84. Eskeland,R., Freyer,E., Leeb,M., Wutz,A. and Bickmore,W.A. (2010) Histone acetylation and the maintenance of chromatin compaction by Polycomb repressive complexes. *Cold Spring Harb. Symp. Quant. Biol.*, **75**, 71–78.
85. Newkirk,S.J., Lee,S., Grandi,F.C., Gaysinskaya,V., Rosser,J.M., Vanden Berg,N., Hogarth,C.A., Marchetto,M.C.N., Muotri,A.R., Griswold,M.D. *et al.* (2017) Intact piRNA pathway prevents L1 mobilization in male meiosis. *Proc. Natl. Acad. Sci. U.S.A.*, **114**, E5635–E5644.
86. Suzuki,J., Yamaguchi,K., Kajikawa,M., Ichiyanagi,K., Adachi,N., Koyama,H., Takeda,S. and Okada,N. (2009) Genetic evidence that the non-homologous end-joining repair pathway is involved in LINE retrotransposition. *PLos Genet.*, **5**, e1000461.
87. Houtkooper,R.H., Pirinen,E. and Auwerx,J. (2012) Sirtuins as regulators of metabolism and healthspan. *Nat. Rev. Mol. Cell Biol.*, **13**, 225–238.
88. Khan,H., Smit,A. and Boissinot,S. (2006) Molecular evolution and tempo of amplification of human LINE-1 retrotransposons since the origin of primates. *Genome Res.*, **16**, 78–87.
89. Sookdeo,A., Hepp,C.M., McClure,M.A. and Boissinot,S. (2013) Revisiting the evolution of mouse LINE-1 in the genomic era. *Mob. DNA*, **4**, 3.
90. Blank,M.F. and Grummt,I. (2017) The seven faces of SIRT7. *Transcription*, **8**, 67–74.
91. Durand-Dubief,M., Sinha,I., Fagerstrom-Billai,F., Bonilla,C., Wright,A., Grunstein,M. and Ekwall,K. (2007) Specific functions for the fission yeast Sirtuins Hst2 and Hst4 in gene regulation and retrotransposon silencing. *EMBO J.*, **26**, 2477–2488.
92. Van Meter,M., Kashyap,M., Rezazadeh,S., Geneva,A.J., Morello,T.D., Seluanov,A. and Gorbunova,V. (2014) SIRT6 represses LINE1 retrotransposons by ribosylating KAP1 but this repression fails with stress and age. *Nat. Commun.*, **5**, 5011.
93. Tasselli,L., Xi,Y., Zheng,W., Tennen,R.I., Odrowaz,Z., Simeoni,F., Li,W. and Chua,K.F. (2016) SIRT6 deacetylates H3K18ac at pericentric chromatin to prevent mitotic errors and cellular senescence. *Nat. Struct. Mol. Biol.*, **23**, 434–440.

94. Sullivan,T., Escalante-Alcalde,D., Bhatt,H., Anver,M., Bhat,N., Nagashima,K., Stewart,C.L. and Burke,B. (1999) Loss of A-type lamin expression compromises nuclear envelope integrity leading to muscular dystrophy. *J. Cell Biol.*, **147**, 913–920.
95. Nikolova,V., Leimena,C., McMahon,A.C., Tan,J.C., Chandar,S., Jogia,D., Kesteven,S.H., Michalicek,J., Otway,R., Verheyen,F. *et al.* (2004) Defects in nuclear structure and function promote dilated cardiomyopathy in lamin A/C-deficient mice. *J. Clin. Invest.*, **113**, 357–369.
96. Solovei,I., Wang,A.S., Thanisch,K., Schmidt,C.S., Krebs,S., Zwerger,M., Cohen,T.V., Devys,D., Foisner,R., Peichl,L. *et al.* (2013) LBR and lamin A/C sequentially tether peripheral heterochromatin and inversely regulate differentiation. *Cell*, **152**, 584–598.
97. Harr,J.C., Gonzalez-Sandoval,A. and Gasser,S.M. (2016) Histones and histone modifications in perinuclear chromatin anchoring: from yeast to man. *EMBO Rep.*, **17**, 139–155.
98. Stierle,V., Couprie,J., Ostlund,C., Krimm,I., Zinn-Justin,S., Hossenlopp,P., Worman,H.J., Courvalin,J.C. and Duband-Goulet,I. (2003) The carboxyl-terminal region common to lamins A and C contains a DNA binding domain. *Biochemistry*, **42**, 4819–4828.
99. Burke,B. and Stewart,C.L. (2013) The nuclear lamins: flexibility in function. *Nat. Rev. Mol. Cell Biol.*, **14**, 13–24.
100. Harr,J.C., Luperchio,T.R., Wong,X., Cohen,E., Wheelan,S.J. and Reddy,K.L. (2015) Directed targeting of chromatin to the nuclear lamina is mediated by chromatin state and A-type lamins. *J. Cell Biol.*, **208**, 33–52.
101. Bruston,F., Delbarre,E., Ostlund,C., Worman,H.J., Buendia,B. and Duband-Goulet,I. (2010) Loss of a DNA binding site within the tail of prelamin A contributes to altered heterochromatin anchorage by progerin. *FEBS Lett.*, **584**, 2999–3004.
102. Hendzel,M.J., Delcuve,G.P. and Davie,J.R. (1991) Histone deacetylase is a component of the internal nuclear matrix. *J. Biol. Chem.*, **266**, 21936–21942.
103. Zink,D., Amaral,M.D., Englmann,A., Lang,S., Clarke,L.A., Rudolph,C., Alt,F., Luther,K., Braz,C., Sadoni,N. *et al.* (2004) Transcription-dependent spatial arrangements of CFTR and adjacent genes in human cell nuclei. *J. Cell Biol.*, **166**, 815–825.
104. Bhaskara,S., Knutson,S.K., Jiang,G., Chandrasekharan,M.B., Wilson,A.J., Zheng,S., Yenamandra,A., Locke,K., Yuan,J.L., Bonine-Summers,A.R. *et al.* (2010) Hdac3 is essential for the maintenance of chromatin structure and genome stability. *Cancer Cell*, **18**, 436–447.
105. Somech,R., Shaklai,S., Geller,O., Amariglio,N., Simon,A.J., Rechavi,G. and Gal-Yam,E.N. (2005) The nuclear-envelope protein and transcriptional repressor LAP2beta interacts with HDAC3 at the nuclear periphery, and induces histone H4 deacetylation. *J. Cell Sci.*, **118**, 4017–4025.
106. Demmerle,J., Koch,A.J. and Holaska,J.M. (2012) The nuclear envelope protein emerin binds directly to histone deacetylase 3 (HDAC3) and activates HDAC3 activity. *J. Biol. Chem.*, **287**, 22080–22088.
107. Gruenbaum,Y. and Foisner,R. (2015) Lamins: nuclear intermediate filament proteins with fundamental functions in nuclear mechanics and genome regulation. *Annu. Rev. Biochem.*, **84**, 131–164.
108. Zink,D., Fischer,A.H. and Nickerson,J.A. (2004) Nuclear structure in cancer cells. *Nat. Rev. Cancer*, **4**, 677–687.
109. Sakthivel,K.M. and Sehgal,P. (2016) A novel role of lamins from genetic disease to cancer biomarkers. *Oncol Rev*, **10**, 309.
110. Ghosh,S. and Zhou,Z. (2014) Genetics of aging, progeria and lamin disorders. *Curr. Opin. Genet. Dev.*, **26**, 41–46.
111. Shah,P.P., Donahue,G., Otte,G.L., Capell,B.C., Nelson,D.M., Cao,K., Aggarwala,V., Cruickshanks,H.A., Rai,T.S., McBryan,T. *et al.* (2013) Lamin B1 depletion in senescent cells triggers large-scale changes in gene expression and the chromatin landscape. *Genes Dev.*, **27**, 1787–1799.
112. Hug,C.B., Grimaldi,A.G., Kruse,K. and Vaquerizas,J.M. (2017) Chromatin architecture emerges during zygotic genome activation independent of transcription. *Cell*, **169**, 216–228.
113. Fadloun,A., Le Gras,S., Jost,B., Ziegler-Birling,C., Takahashi,H., Gorab,E., Carninci,P. and Torres-Padilla,M.E. (2013) Chromatin signatures and retrotransposon profiling in mouse embryos reveal regulation of LINE-1 by RNA. *Nat. Struct. Mol. Biol.*, **20**, 332–338.
114. Jachowicz,J.W., Bing,X., Pontabry,J., Boskovic,A., Rando,O.J. and Torres-Padilla,M.E. (2017) LINE-1 activation after fertilization regulates global chromatin accessibility in the early mouse embryo. *Nat. Genet.*, **49**, 1502–1510.
115. De Cecco,M., Ito,T., Petrashen,A.P., Elias,A.E., Skvir,N.J., Criscione,S.W., Caligiana,A., Brocculi,G., Adney,E.M., Boeke,J.D. *et al.* (2019) L1 drives IFN in senescent cells and promotes age-associated inflammation. *Nature*, **566**, 73–78.
116. Simon,M., Van Meter,M., Ablaeva,J., Ke,Z., Gonzalez,R.S., Taguchi,T., De Cecco,M., Leonova,K.I., Kogan,V., Helfand,S.L. *et al.* (2019) LINE1 derepression in aged Wild-Type and SIRT6-Deficient mice drives inflammation. *Cell Metab.*, **29**, 871–885.